

RESEARCH ARTICLE

10.1002/2015JB012174

Key Points:

- Deformation of Chi-Chi thrust termination is delineated and analyzed
- Width variation of Chi-Chi deformation zone was attributed to fault branching
- Fault propagation at shallow depth

Supporting Information:

- Supporting Information S1

Correspondence to:

W.-J. Huang,
huang22@ncu.edu.tw

Citation:

Huang, W.-J., W.-S. Chen, Y.-H. Lee, C.-C. Yang, M.-L. Lin, C.-S. Chiang, J.-C. Lee, and S.-T. Lu (2016), Insights from heterogeneous structures of the 1999 M_w 7.6 Chi-Chi earthquake thrust termination in and near Chushan excavation site, Central Taiwan, *J. Geophys. Res. Solid Earth*, 121, doi:10.1002/2015JB012174.

Received 1 MAY 2015

Accepted 8 NOV 2015

Accepted article online 17 NOV 2015

Insights from heterogeneous structures of the 1999 M_w 7.6 Chi-Chi earthquake thrust termination in and near Chushan excavation site, Central Taiwan

Wen-Jeng Huang¹, Wen-Shan Chen², Yuan-Hsi Lee³, Chih-Cheng Yang⁴, Ming-Lang Lin⁵, Cheng-Shing Chiang⁶, Jian-Cheng Lee⁷, and Shih-Ting Lu⁸

¹Graduate Institute of Applied Geology, National Central University, Jhongli City, Taiwan, ²Department of Geosciences, National Taiwan University, Taipei, Taiwan, ³Department of Earth and Environmental Sciences, National Chung Cheng University, Chiayi, Taiwan, ⁴Exploration and Development Research Institute, Chinese Petroleum Company, Miaoli, Taiwan, ⁵Department of Civil Engineering, National Taiwan University, Taipei, Taiwan, ⁶National Museum of Natural Science, Taichuang, Taiwan, ⁷Institute of Earth Sciences, Academia Sinica, Taipei, Taiwan, ⁸Central Geological Survey, MOEA, New Taipei City, Taiwan

Abstract We describe and analyze the surface and subsurface deformation of the 1999 Chi-Chi earthquake thrust termination of the Chelungpu fault in and near the Chushan excavation site, central Taiwan. In order to minimize damage to engineering structures within a deformation zone and formulate regulations for earthquake fault zones and fault setbacks, one needs to know the characteristics of the deformation zone and the connection between surface and subsurface deformation. The surface deformation zone of high strain induced by the earthquake faulting ranges from 15 to 70 m in width, and characterized by a 0.5 to 2 m high escarpment is much wider in the hanging wall. Exposures in the trench, 40 m long and 10 m deep, excavated across the earthquake ground rupture, show on the one hand the heterogeneous structure of a steep, monocline-like fold. On the other hand, strikingly different surface deformation profiles on either side of the 14 m wide trench, i.e., semiparabola-like and monoclinical, do not reflect in any obvious way the subsurface structure. The analysis of our detailed mapping results along with well logs suggests that the significant width variation of the surface deformation zone is attributed to secondary faults branching from the dominant fault at several tens of meters depth. The surface profile of the escarpment is controlled by the depth of the relevant fault tip, and the subsurface heterogeneous structure formed during at least four earthquakes.

1. Introduction

The 1999 Chi-Chi earthquake in Taiwan introduced earthquake geologists to two phenomena of ground rupture associated with thrust faulting that had been uncommonly observed previously. Taiwanese geologists noted early in their field investigations that one rarely observed a fault in the escarpment at the leading edge of a thrust. Rather, one commonly observed a monoclinical escarpment [*Taiwan Central Geological Survey [TCGS], 1999a, 1999b; Huang et al., 2000; Lee et al., 2001; Chen et al., 2001b*]. The heights of monoclinical escarpments ranged from 10 m in the north to 1 m in the south over the 80 km length of the N-S part of the Chi-Chi rupture [*Chen et al., 2001a; Lee et al., 2003; Lin et al., 2003*]. The second feature recognized in a few places is that there can be a broad ground deformation zone associated with the escarpment. Although the most intense deformation typically occurred at the escarpment, there was noticeable deformation nearby, especially in the hanging wall of the thrust. The deformation caused much of the damage to dwellings, large structures, and infrastructure of communities through which the rupture passed [*Lin and Suen, 2000; Dong et al., 2004*].

Deformation zones and damage along coseismic ruptures were recognized in 1906 San Francisco earthquake [*Gilbert, 1907; Lawson, 1908*] and were noticed by a few investigators in the 1990s [e.g., *Martosudarmo et al., 1997; Johnson et al., 1993, 1994, 1996*]. They were also mentioned by *Huang et al. [2000], Rubin et al. [2001], Kelson et al. [2001], Johnson et al. [2002], Rockwell et al. [2002], Klinger et al. [2005], Kaneda et al. [2008], Lin et al. [2009], Huang and Johnson [2010], Ren et al. [2010], and Li et al. [2010]*. Many studies have addressed particular structures of ground deformation occurring during the Chi-Chi earthquake [e.g., *Lee et al., 2002, 2005; Lee and Shih, 2011*] or generalized structure patterns along the 100 km long Chi-Chi deformation zone [e.g., *Chen et al., 2001b; Lin et al., 2001, 2003; Ouchi et al., 2001*].

To our knowledge, only a few studies [Kelson *et al.*, 2001; Huang, 2006; Ota *et al.*, 2007] mapped and analyzed the Chi-Chi deformation zone in great detail or even other earthquake deformation zones elsewhere [e.g., Tchalenko and Ambraseys, 1970; Philip and Meghraoui, 1983; Johnson *et al.*, 1994; Treiman *et al.*, 2002; Klinger *et al.*, 2005; Lin and Nishikawa, 2011]. Mechanical models have been proposed to explain the formation of deformation zones [Johnson *et al.*, 2002; Huang and Johnson, 2010]. In addition, centrifuge experiments along with discrete element analyses [Chang *et al.*, 2013, 2015] were used to model reverse fault slip and estimate the width of induced surface deformation zones for various fault dips. Detailed mapping of coseismic ground surface ruptures complemented by excavations across the fault zone (Chushan trench) benefits both modelers and experimentalists. It helps scientists understand how an earthquake thrust faulting may deform the ground surface and interact with engineering structures and how the fault propagates through the geomaterials. Meanwhile, it helps governments to delineate zones of surface fault-rupture hazard, formulate regulations for earthquake fault zones and fault setbacks, and encourage landowners to avoid fault zones for land development [e.g., Bryant and Hart, 2007; Boncio *et al.*, 2012; Villamor *et al.*, 2012].

Shortly after the Chi-Chi earthquake, we investigated the surface deformation at Tanliwun area where the Chushan trench is located. In 2005, we mapped surface deformation in the hanging wall using a total station theodolite. The trench was excavated in 2002, and its exposures were laterally expanded twice in 2005 and 2012, respectively. We mapped the subsurface structures beneath the coseismic escarpment at scales of 1:10 to 1:20 several times as the trench was expanded and reexcavated and has two well logs adjacent to the trench. Thus, we have firsthand detailed information for both surface and subsurface deformation. This study aims at documenting the surface and subsurface deformation at thrust termination, analyzing the deformation in different scales from decameters to centimeters, and discussing how and why the structures evolved and were interrelated laterally and temporally, and we propose possible mechanisms or reasons for the formation of these structures.

2. Geology and Ground Deformation Near the Chushan Excavation Site, Tanliwun Area

The 1999 Chi-Chi earthquake ground rupture is generally near the western edge of the Western Foothills, the foothills of the Hsuehshan Range. The foothills range in altitude up to 1000 m and comprise largely Oligocene to Pleistocene strata [Chou, 1973, 1980; Huang and Cheng, 1983]. The altitude of the Hsuehshan Range is up to about 4000 m. It contains thick, continuous Eocene to Miocene formations [Chen, 1977; Ho, 1988; Teng *et al.*, 1991]. Figure 1 shows the entire Chi-Chi rupture following the Chelungpu fault, one of three long-recognized active east dipping thrust faults in western Taiwan [Shyu *et al.*, 2005]. About 80 km of the trace of the Chi-Chi rupture trends N-S and mostly coincides with the topographic front of the Western Foothills. The trace of the northern 20 km of the Chi-Chi rupture trends ENE across the Western Foothills (Figure 1).

The Chushan trench was excavated in November 2002 in the Tanliwun area, in the southern part of the Chi-Chi earthquake ground rupture, approximately 5 km south of the Chuoshui River and 5 km north of Chushan town (Figure 1). The trench remained open for 3 years and was filled in 2005. In late 2012, it was reopened as an exhibition in the Chelungpu Fault Preservation Park. There are two terraces in the Tanliwun area with a 5 m difference in altitude between them (Figure 2). The lower terrace has an altitude of approximately 148 m above sea level; it is about 3 m higher than the Coastal Plain. The Coastal Plain is mostly covered by Quaternary fluvial strata and underlain by about 2000 m of Pliocene strata that occur at depths between 1500 to 3500 m [Chou, 1971, 1999]. The hills adjacent to Tanliwun village range from 150 to 600 m above the lower terrace and comprise of Pliocene shallow marine strata. The Chushan trench was excavated on the lower terrace, about 50 m west of the front of the Western Foothills. Holocene cobbly gravels were exposed at the base of the trench, in the hanging wall, and also appeared in two drill sites at shallow depths (Figure 2).

We collated the data from different sources including our own field observation shortly after the Chi-Chi earthquake, earthquake rupture maps at a scale of 1:1000 with 1 m interval topographic contour lines, produced by Taiwan Yung-Cheng engineering consultants in April of 2000, two versions of Orthophoto basemaps at a scale of 1:5000 made from aerial photographs taken before and after the earthquake, in July 1998 and November 1999, respectively. The integrated results of the surface deformation investigation

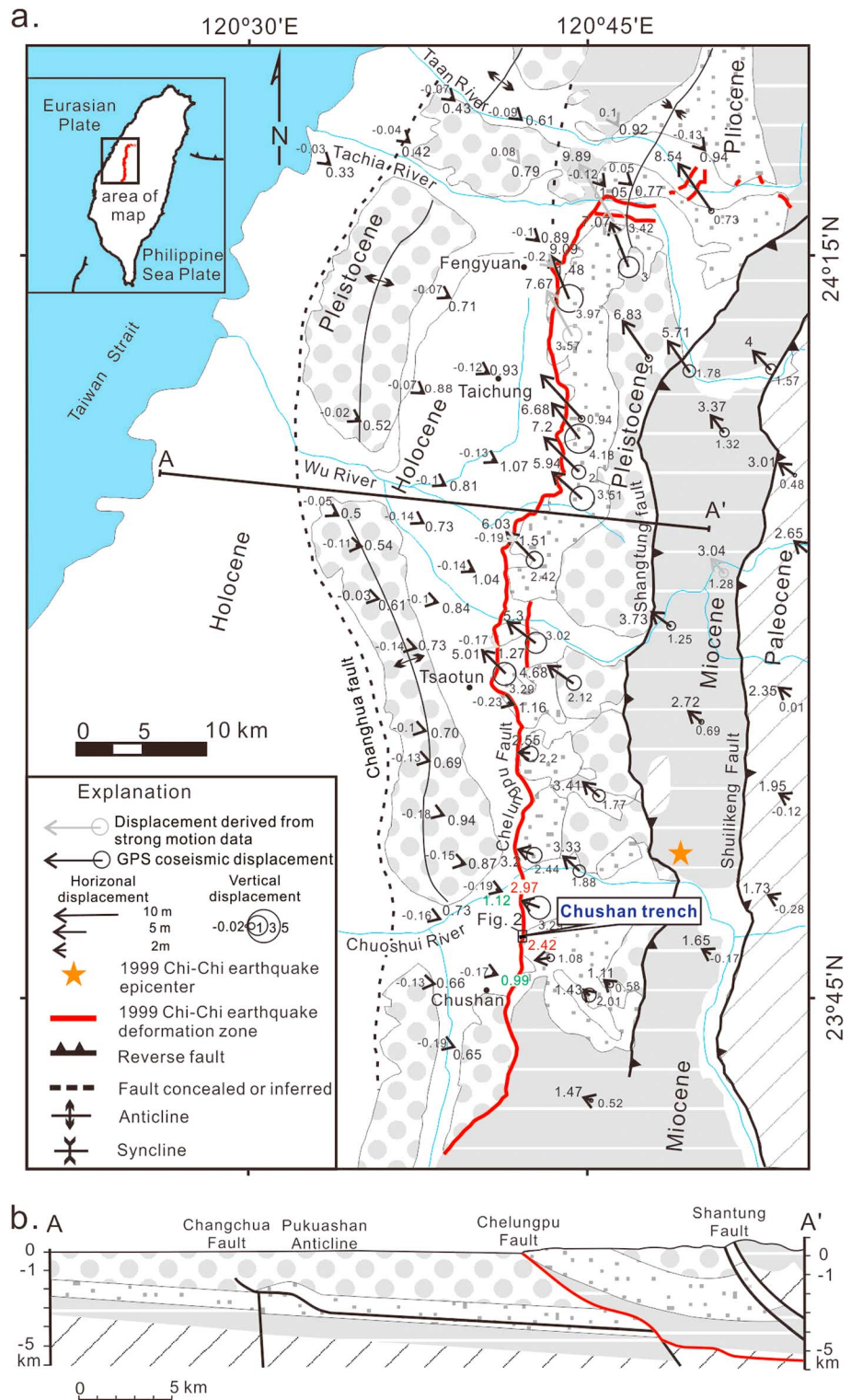


Figure 1. Regional geologic setting of the Chi-Chi rupture in west-central Taiwan. (a) Most active faults in west-central Taiwan (modified from Lin et al. [2002]). The Chi-Chi rupture is generally considered to be the surface trace of a reactivation of the Chelungpu fault. The Chushan trench in the southern part of the area is named after the city of Chushan, 5 km SW of Taniwun village. (b) Geological cross section (modified from cross sections by Chou and Yang [1986] and Angelier et al. [2000]). All stratigraphic units tend to thicken eastward. A thin wedge of Miocene rocks was thrust onto the Pliocene and Pleistocene sediments along the Chelungpu fault. Displacements are derived from strong motion data and GPS surveys before and after the Chi-Chi earthquake (data from Yu et al. [2001]).

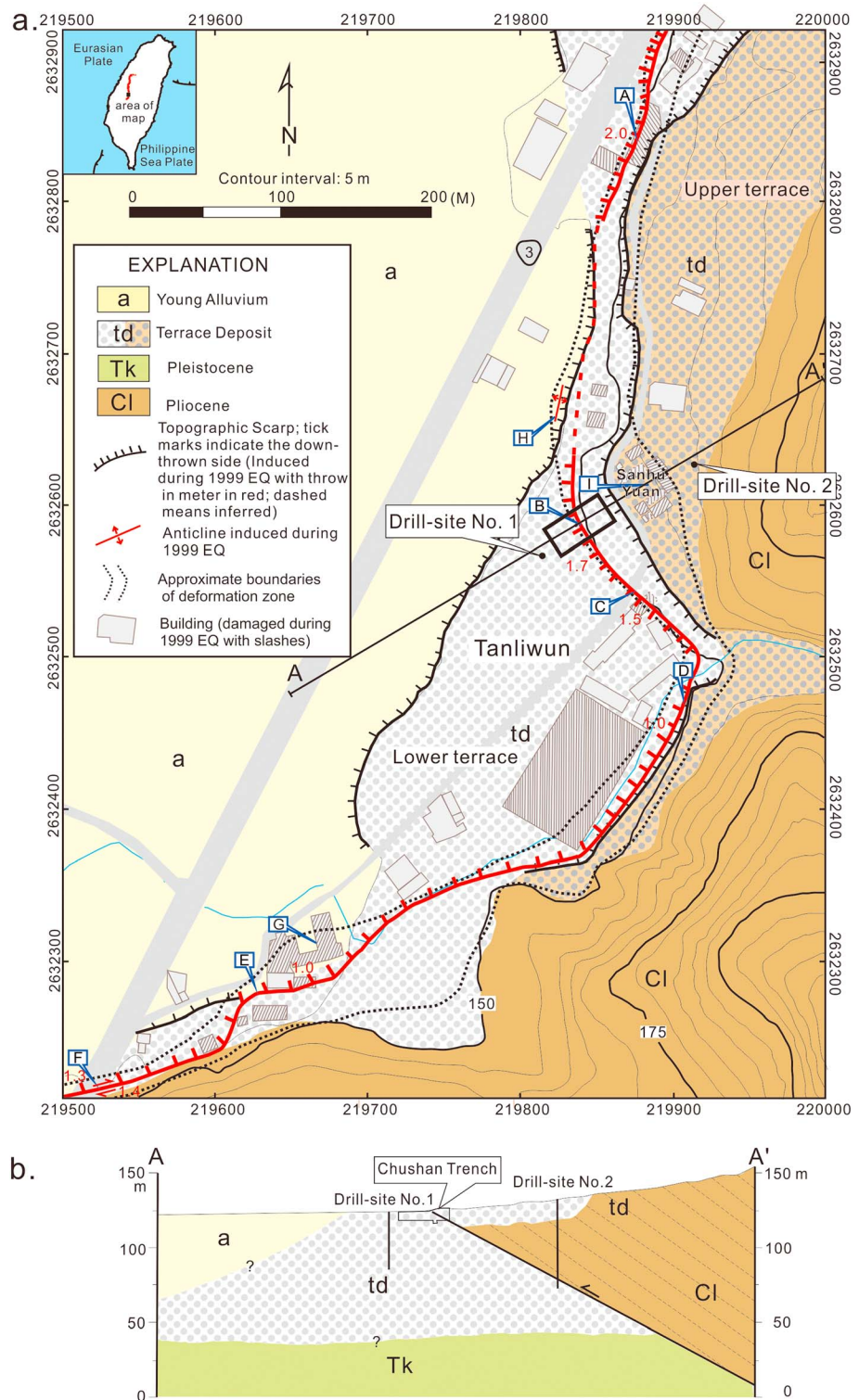


Figure 2. Local geologic setting of the Chushan trench at the Tanliwun village (trench location shown in Figure 1). (a) Local geologic map. Capital letters in blue frame indicate the location of photographs in Figures 4, 5, and 7. Coordinates are in TWD97. Note that houses collapsed during the Chi-Chi earthquake and removed shortly after the earthquake are not shown. The base map is an orthophoto map at a scale of 1:5000 made from aerial photographs taken after the earthquake in November 1999. (b) Cross section along the Chushan trench axis.

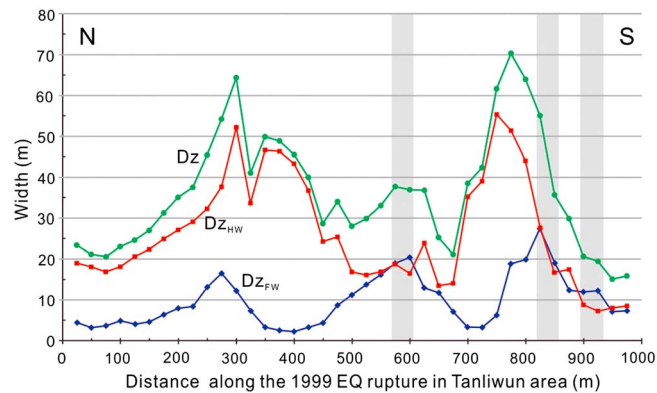


Figure 3. Width variation of deformation zone (Dz) in the Tanliwun area. Dz boundary in the hanging wall at the shaded parts was poorly constrained because of steep slope and dense vegetation right next to the 1999 earthquake rupture. The subscripts HW and FW mean hanging wall and footwall, respectively. The two Dz peaks occur near location B and G in Figure 2.

are summarized in Figure 2. The solid red line with tick marks is the location of the escarpment formed during the 1999 Chi-Chi earthquake. The two dotted lines in Figure 2 are estimated boundaries of the ground deformation zone. The deformation zone, characterized by a 0.5 to 2 m high escarpment, roughly trends along the toe of the hills. It ranges in width from 15 to 70 m and is highly asymmetrical relative to the toe of the escarpment and is most of all, much wider in the hanging wall than in the footwall (Figure 3). Note that the escarpment is mainly located on the lower terrace, but the deformation zone was not restricted to the lower terrace. Below, we describe the features within the deformation zone along an approximately 1.0 km long stretch in the Tanliwun area, moving from north to south across Figure 2.

are summarized in Figure 2. The solid red line with tick marks is the location of the escarpment formed during the 1999 Chi-Chi earthquake. The two dotted lines in Figure 2 are estimated boundaries of the ground deformation zone. The deformation zone, characterized by a 0.5 to 2 m high escarpment, roughly trends along the toe of the hills. It ranges in width from 15 to 70 m and is highly asymmetrical relative to the toe of the escarpment and is most of all, much wider in the hanging wall than in the footwall (Figure 3). Note that the escarpment is mainly located on the lower terrace, but the deformation zone was not restricted to the lower terrace. Below, we describe the features within the deformation zone along an approximately 1.0 km long stretch in the Tanliwun area, moving from north to south across Figure 2.

2.1. The Main Feature: The Escarpment

In the upper right of Figure 2, at location A, the escarpment of the deformation zone trends NNE to SSW (Figure 4a). Before the Chi-Chi earthquake, the ground surface in this neighborhood was flat. After the earthquake, the floor of the storage shed was uplifted on a 2 m high monoclinical escarpment. The shed was distorted, and some of the foundation piers supporting the columns of the building were exposed. The escarpment extended southward tens of meters from location A. We could not trace the escarpment all the way to location B (Figure 2) because of dense vegetation and a steep slope associated with the riser between the lower terrace and the Coastal Plain.

At location B (Figure 2), we again see the escarpment (Figure 4b, photograph taken in November 2002, 3 years after the earthquake) as a warp across a field where the Chushan trench was excavated. The eastern side of the field was uplifted about 1.7 m [Chen et al., 2007], and a monoclinical escarpment formed during the earthquake. The deformation zone was oriented quite differently here from that at location A. The strike changes almost 90° to NW. The escarpment continued with the new trend and intertwined with the northern wall of the light-toned building visible in the background of Figure 4b and on the right-hand side of Figure 4c (location C, Figure 2). By the time the photograph in Figure 4c was taken, the road over the escarpment had been smoothed out for traffic so only the height of the escarpment was visible there. Before the earthquake, the road came down a gentle, SW facing slope toward the foreground. Also, there was an open space several meters wide between the light-toned building on the right and the betel-nut tree grove behind the building. After the earthquake, the ground in the background of Figure 4c had been uplifted about 1.5 m and pushed several meters toward the building.

South of the creek near location D (Figure 2), the trend of the escarpment changes from NW to NE. The foundation of a concrete bridge across the creek was damaged and displaced about 1.0 m on either side of the creek. Figure 4d is a southeast view of the escarpments. The upper escarpment in the background is the riser of the upper terrace. The lower escarpment, approximately 1.0 m high, was formed during the Chi-Chi earthquake. Its trend can be recognized by the lineament of tilted betel-nut trees.

Farther south, the escarpment trends roughly ENE in the southernmost one-third (Figure 2). At location E, the floor of the barn used to be at the same level as the cement slab in the foreground before the earthquake (Figure 4e). After the earthquake, the ground had been uplifted about 1.0 m. A pipeline was broken, and an electric pole was tilted by the deformation. Figure 4f shows the earthquake damage on Province Road 3 at location F (Figure 2). The road surface was flat prior to the earthquake. During the earthquake, the southern side was uplifted 1.3 m and displaced 1.4 m in the right-lateral sense, as shown on right edge of photo.



Figure 4. Chi-Chi earthquake-induced escarpments in the Taniwun area (locations shown in Figure 2). Detailed description of each escarpment refers to the text.

2.2. Deformation in the Footwall in Front of the Escarpment

In no place along the escarpment in the Taniwun area have we thus far observed deformation features west of the escarpment in the footwall of the fault. The ground has been essentially undeformed there. In particular, the only damage to the building shown in Figures 4b and 4c is related to the main escarpment itself, which toe pushed in the back wall of the light-toned building. The damage did not extend farther into the building or into the courtyard associated with the building (Figure 2c). Very limited footwall deformation was observed in the Chushan trench. Thus, our observations thus far suggest that if there is a wide deformation zone along the Taniwun trace, the deformation zone is asymmetrical: it is bounded on the west by an escarpment.

Ground deformation in the footwall was observed at only two locations G and H (Figure 2). At location G, two fractures appeared in the courtyard of a U-shaped house (Figure 5a) 20 m NW of the escarpment, which was 1.0 m high. The fractures and flexures in the asphalt pavement indicate thrusting, with the ground in the hanging wall moving relatively toward the NW, similar to the main escarpment itself. Thrusting extended laterally and damaged the house. The amount of uplift by thrusting in the pavement, though, was on the order of 20 to 40 cm. There was no damage or visible deformation in the asphalt pavement to the north of the two fractures, neither in between the south fracture and the main escarpment.

The other location is 50 m northwest of the trench site (location H in Figure 2). The ground surface was deformed as an elongated dome with a hinge line parallel to the escarpment at the western edge of the lower terrace. Figure 5b is a northeast view of the dome, which could be recognized thanks to a lineament of tilted betel-nut trees. Note that the betel-nut trees were inclined in an opposite direction on the opposite limbs of the anticlinal dome.



Figure 5. Geological features in the footwall induced by Chi-Chi earthquake faulting. (a) Two fractures and flexures appeared in the courtyard of a house (location G, Figure 2). The amount of uplift by thrusting in the pavement was on the order of 20 to 40 cm. (b) Northeast view of an anticlinal dome (location H, Figure 2). The betel-nut trees were inclined in an opposite direction on the either limb of the dome. The toes of the anticlinal dome are highlighted in red with tip marks, which indicate the down-thrown side.

that the maximum compression in the asphalt and probably in the ground at the time the cracks formed was in that direction [Cotterell and Rice, 1980]. Some of the fractures look like a sickle in shape and accommodated lateral slip along the straight parts of their traces. The amount of slip was small, everywhere less than 2 cm. Along the curved part of sickle-like fractures, the sides were pushed and uplifted toward each other (Figure 6b). They are well-defined compression or thrust features, which also indicate compression in the NE-SW direction.

Brick house H6 was bent, distorted, and cracked (Figure 7a). We used an electronic theodolite (Wild T1000) to measure the bending along the floor of the porch and the line between the green and white painted walls (Figure 7a). The survey (Figure 7b) shows that the middle of the house was relatively elevated about 28 cm, while the eastern end of the house was relatively elevated about 18 cm in reference to the western end. The uplift of the house H6 along an axis oriented NW-SE may well be a result of a thrust fault that accommodated small thrust offset. Perhaps the small thrust fault or other thrust faults were beneath the broad domes in the courtyard. In any case, the structures in the asphalt in the courtyard and the deformation within house H6 clearly reflect thrusting resulting from NE-SW compression in the Sanhu Yuan, which is consistent with thrusting in the Chushan trench during the 1999 earthquake.

3. Deformation Exposed on Walls of the Chushan Trench Crossing on Fault Zone

3.1. Setting and Exposures of the Trench

Prior to the 1999 earthquake, the ground at the site of the Chushan trench was an essentially flat building site, sloping gently SW. There was a one-storey brick building with a yard and a vegetable garden at the site.

2.3. Deformation of a Homestead in the Hanging Wall

Typically, the deformation in the hanging wall was much wider than the deformation in the footwall (Figures 2 and 3). The damage of buildings and floors within the deformation zone was much more severe in the hanging wall. A Sanhu Yuan (location I, Figure 2), a type of traditional, rural Taiwanese homestead is about 40 m northeast of the Chushan trench (Figure 2). It was damaged by the Chi-Chi earthquake and is in the hanging wall of the faults exposed in the Chushan trench.

The courtyard of the Sanhu Yuan was a flat surface of asphalt prior to the earthquake, used for drying harvested rice. The earthquake caused the asphalt to become bumpy and fractured. The diameters of the bumps are on the order of 5 to 15 m. The maximum relief of the bumps reaches 40 cm (Figure 6b). Most of the fractures are open (Mode I) cracks and are oriented roughly NE-SW. Crack openings are 0.5 to 1 cm on average. The openings narrow toward to the ends. The maximum opening within the fractures is 5 cm. Some fractures extend several decimeters into the ground. The typical shapes of the crack walls are zig-zag. The traces of the cracks are preferentially oriented about NE-SW, indicating

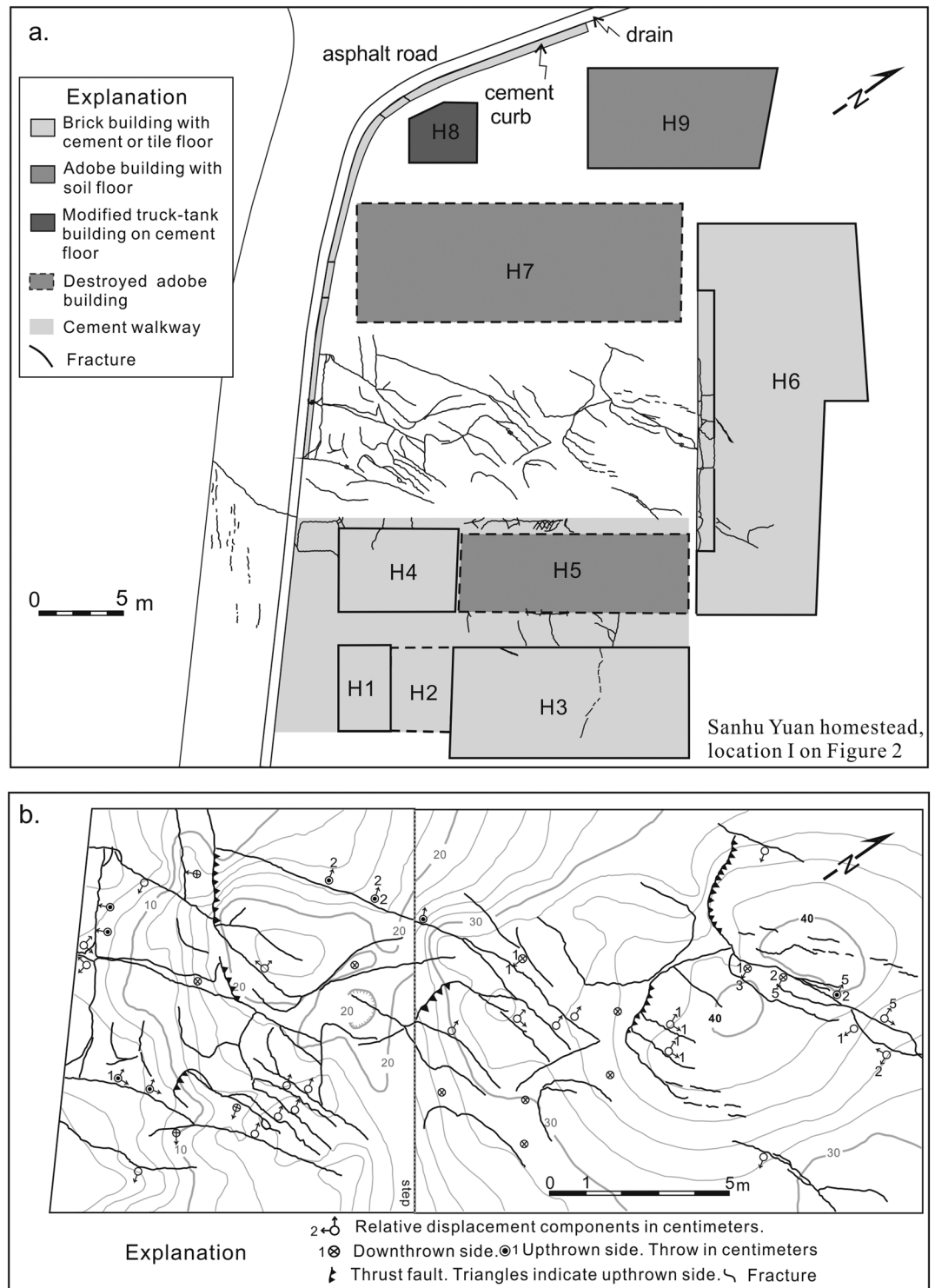


Figure 6. Deformation of a Sanhu Yuan, traditional Taiwanese homestead, in the hanging wall. (location I, Figure 2) (a) Building setting and traces of fractures in the homestead. (b) Topography (contour interval 2 cm) and traces of fractures in the courtyard (contour interval 2 cm). The courtyard was paved with asphalt.

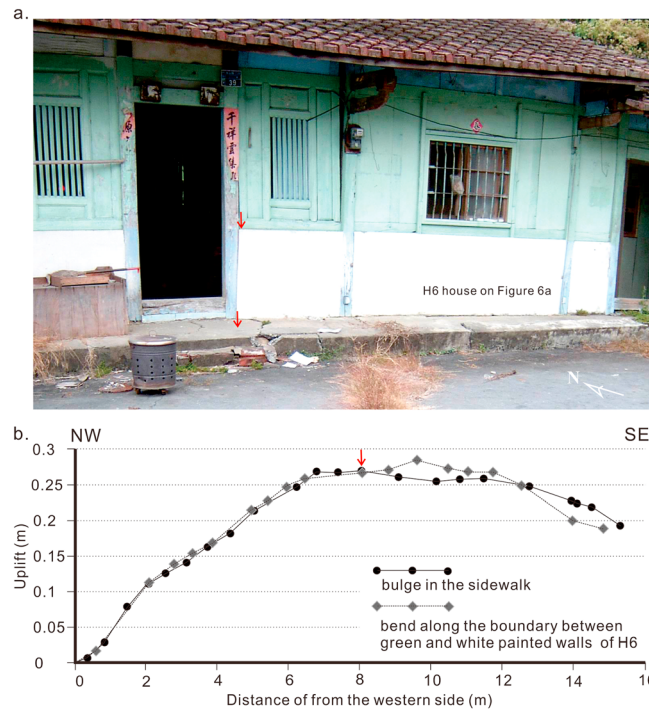


Figure 7. Example of a damaged building in the Sanhu Yuan. Red arrows indicate measurement locations. (a) Northeast view of the building (house H6 in Figure 6). (b) Survey of the deformation along markers that were horizontal prior to the earthquake.

During the earthquake, the trace of an escarpment passed through the site of the house and the formation of the escarpment destroyed the house. The ground surface at the escarpment appeared as a low warp (Figures 4b and 8b).

The Chushan trench was excavated with its long axis passing through the escarpment (Figure 8c); it is up to 10 m deep, 40 m long, and 14 m wide. The sedimentary units exposed in the trench are described in Figure 9. We largely follow the terminology of soils used by geotechnical engineers to focus on the mechanical properties of the soils in the trench. Table 1 shows the engineering properties of the soil samples, which were collected from the sedimentary units. Most units in the trench, except the man-made fill Unit 0 and the cobbly gravel Unit 8, are fine-grained, determined by sieve and hydrometer analyses of all samples. All samples passed through the 4.75 mm sieve (no. 4) so the coarsest grain size is sand as defined by the United Soil Classification System

(USCS D 2487–00). All samples are dominated by silt-sized clasts, the percentages of which range from 55 to 70% (by weight).

According to *Chen et al.* [2003, 2007], the sediments of the lowest unit, Unit 8, represent a fluvial depositional environment recorded by the thick-bedded deposits of mostly quartzite boulders and cobbles in gravel carried from the Central Range by the ancestral Chuoshui River. They indicate that most of the overlying fine-grained sediments are sandy, clayey silt, or clayey, sandy silt. These units were probably deposited as slope wash and as sediment in small tributary streams [*Chen et al.*, 2007]. Unit 3 appears to contain several paleosols. Unit 1 is modern topsoil.

3.2. Structures in the Trench

The Chushan trench exposes two main faults displacing the sedimentary units and the fault-related folds flexing the sedimentary units. These features are exposed on both walls within a 5 to 10 m wide zone separating the hanging wall block from the footwall block, both with essentially horizontal bedding (Figure 10a).

We mapped both walls of the trench. The face above each bench was mapped at scales of 1:10 to 1:20. Those maps were compiled onto a base diagram, showing the benches and faces, internal sedimentary structures within stratigraphic units, and traces of faults throughout the north and south walls of the trench. The deformation mechanism is faulting, as shown in Figure 10c. Figure 10c aims at showing the large-scale structures, including the orientations and positions of the fault traces, as well as an idea of the amount of offset accommodated by the fault. Note that the amount of offset was measured based on faulted markers. In the following, we first describe the main structures, namely, the two main faults and the fault-related fold. Then, we describe secondary features and quantify their significance in accommodating deformation.

3.2.1. Two Main Faults

The trace of the upper main fault (labeled U in Figure 10, right) in the south wall ranges from a very thin line to a 15 cm wide zone; it separates distinctly different sedimentary layers. The fault dips at a shallow angle near the ground surface, but the dip increases to about 35° at a depth of 2 to 3 m and is constant at greater depths. The upper main fault was obviously active in 1999 because it cut through the topsoil to the ground surface.

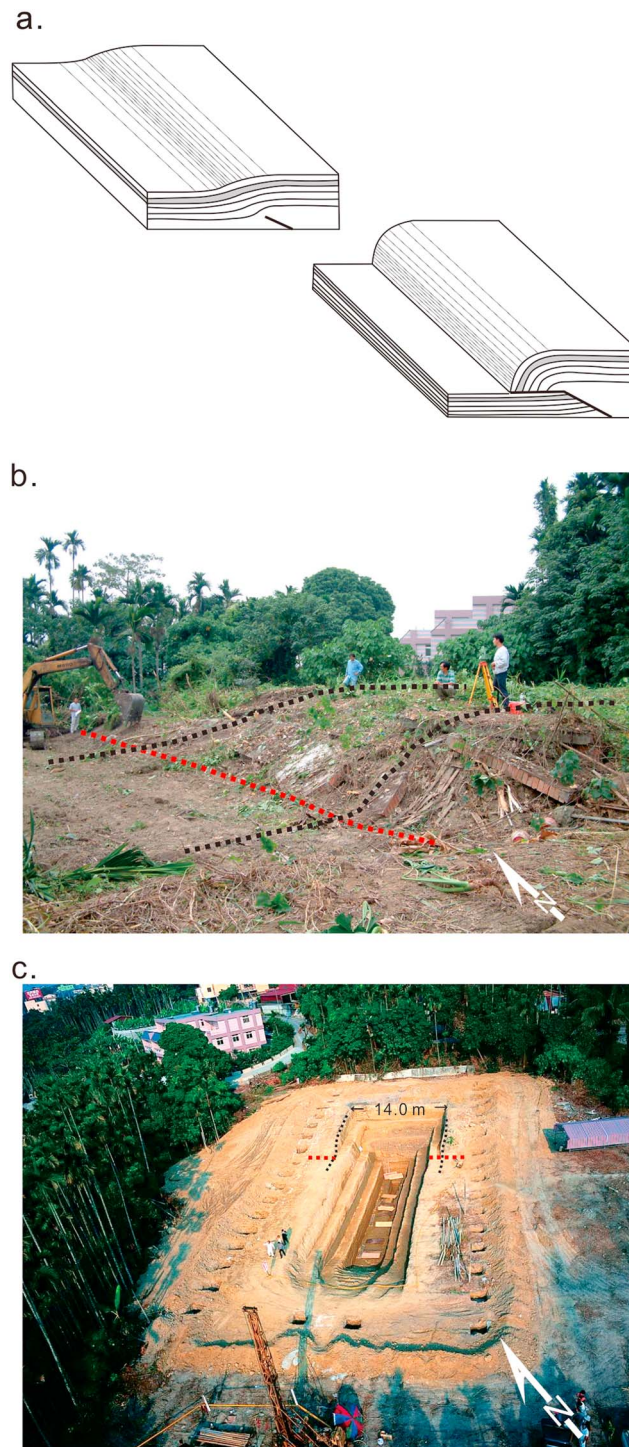
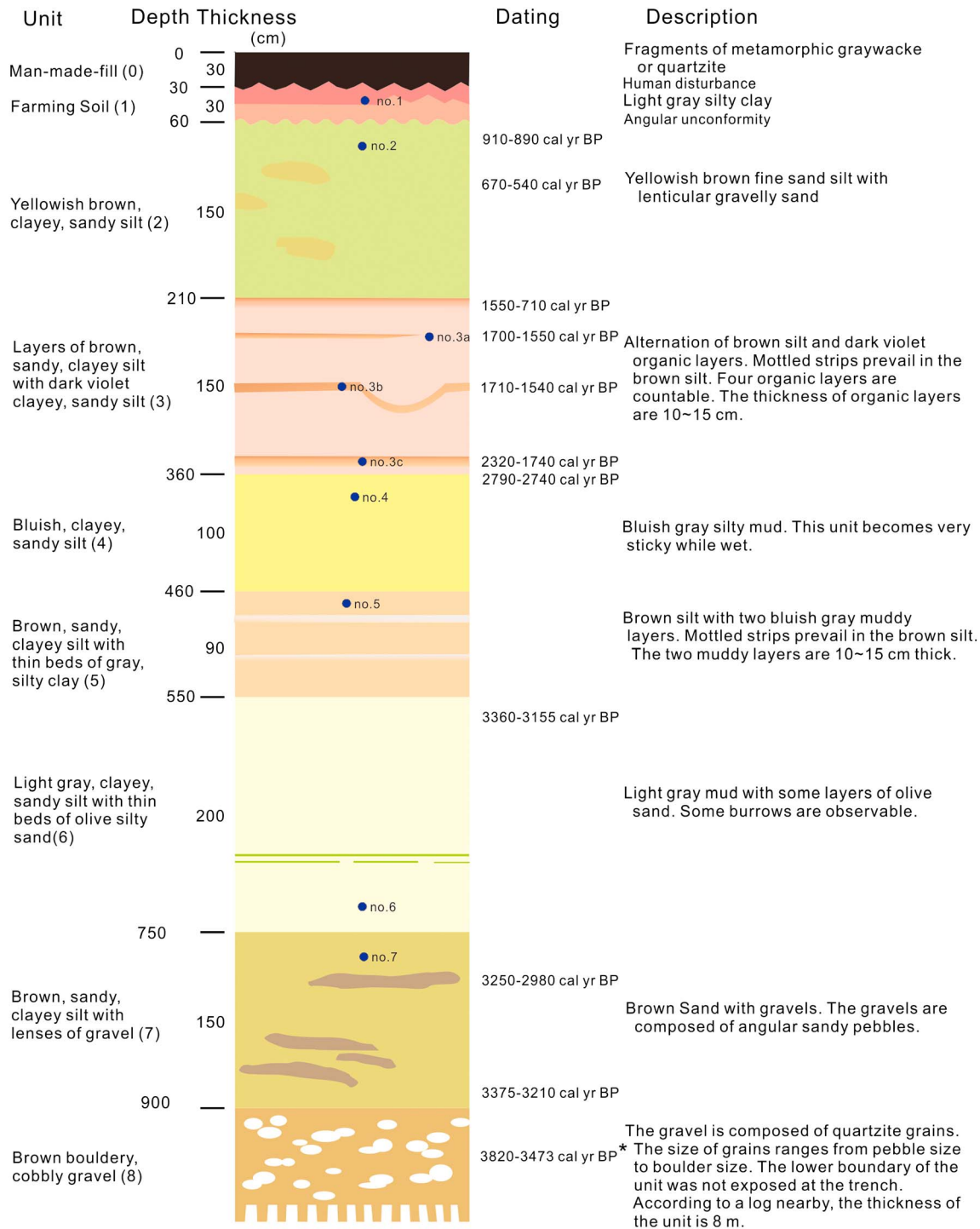


Figure 8. (a) Two idealized forms of escarpments. The subsurface structure is hypothetical. Profile of semiparabola-like thrust-escarpment or toe (lower right). Profile of monoclinal fold-escarpment (upper left). (b) The field in which the Chushan trench was excavated and the 2 m escarpment at the leading edge of the Chi-Chi earthquake rupture. The black dotted lines indicate the approximate location of the upper trench walls and mark the difference in shape of the ground surface. (c) Oblique aerial view toward NE of the Chushan trench in the village of Tanliwun, Taiwan. The toe trace of the escarpment is shown with a red dotted line in Figures 8b and 8c (provided by Wen-Shan Chen, National Taiwan University).

The total offset on this fault is consistently about 4.2 m for Units 6, 7, and 8 (Figures 10b and 10c, right). The upper main fault is not observed in the north wall. It is visible in the lower left in Figure 10a (right) but terminates laterally toward the north face within the gravel (Unit 8) exposed in the NE wall of the trench. Along its trend, within the NE end of the trench, is a flexure defined by reoriented pebbles and a bend in the contact between the gravel and the overlying silt, Unit 7 (Figure 10a, left). The contact appears to be conformable in the flexure. Thus, the upper main fault definitely did not extend to the ground surface in the north wall. Instead, it terminated between the south and north walls of the trench.

The lower main fault (labeled L in Figure 10, left) carries its largest apparent slip in the north wall of the Chushan trench, but it can be traced from the north wall into the south wall of the trench. The apparent dip increases with depth, reaching a maximum apparent dip of 27°. The maximum offset is approximately 2.9 m near the NE end of the north wall (Figure 10c, left). The same offset was measured along the upper branch of the near-horizontal part of the fault (Figure 10c, left). As the lower main fault flattens, it is expressed as at least three branch faults, subparallel to bedding (Figure 10, left). An offset of 1.7 m was measured along just the upper branch, labeled L_u (Figure 10c, left). The middle and lower branches, labeled L_m and L_l , respectively, were judged to have carried only small offsets. The trace of the upper branch L_u has a complicated, digitated form so the upper L_u and middle L_m branches may well have been dormant during the 1999 earthquake. The trace of the lower branch L_l appears to have been active during the 1999 earthquake based on the abruptly truncated roots; however, it likely has accommodated only a few cm of slip. Thus, it may well be that the offset on the lower fault decreases distally along the subhorizontal part of the fault trace in the north wall of the trench (Figure 10c, left).



* Note: the sample collected from fluvial terrace deposits near the trench site and interpreted to be correlative with unit 8.

Figure 9. Stratigraphic column of the Chushan trench. Radiocarbon dates in calibrated years before present (B.P.) (dates from *Chen et al.* [2007]). The dates are written near to equivalent levels of the soils where charcoal was collected. Soil samples nos. 1 to 7 in Table 1 are labeled on equivalent levels of the soils where they were collected.

Table 1. Engineering ^aProperties of Samples of Sedimentary Layers

Soil Unit		1	2	3			4	5	6	7
Sample No.		1	2	3a	3b	3c	4	5	6	7
Grain size analysis (sand: 0.063–2 mm, silt: 0.002–0.063 mm, clay: <0.002 mm)	San (wt %)	24.90	21.70	21.70	31.10	20.50	14.00	27.10	9.00	26.20
	Silt (wt %)	70.10	68.20	68.34	54.40	63.88	69.16	54.97	65.08	57.92
	Clay (wt %)	5.00	10.1	9.96	14.5	15.6	16.8	17.9	25.9	15.9
Water content (ϕ)		14.6	12.9	12.5	12.7	19.4	26.3	22.8	27.9	18.6
^b LL. (ϕ)		34.1	27.5	26.9	24.6	32.1	36.2	31.6	37.3	26.6
LL. (burned; ϕ)		32.0			22.2	28.5				
^b PL. (ϕ)		17.3	19.3	16.6	15.9	14.2	17.0	16.3	16.5	13.6
^b PI. (ϕ)		16.8	8.2	10.3	8.8	17.9	19.2	15.3	20.8	12.9
^c Activity		3.35	0.81	1.04	0.60	1.15	1.14	0.85	0.80	0.81
^b Avg. S. G.		2.65	2.73	2.66	2.70	2.70	2.75	2.67	2.72	2.69

^aNote about the symbol: ϕ . Many of the numbers in the table that appear to be percentages are, in fact, not. By the unconventional convention in Geotechnical Engineering, “percentage” indicates a quantity calculated by dividing the weight of one material by the weight of another material and multiplying by 100!

^bLL.: liquid limit; PL.: plastic limit; PI.: plastic index; Avg. S. G.: average specific gravity.

^cActivity is the ratio of Plasticity Index of a soil to the percent of clay-size particles in the soil (clay-size is finer than 2 μ m). The activity generally reflects the clay mineralogy of the clay-size fraction of a soil [Seed *et al.*, 1964a, 1964b].

The lower main fault can be traced downward along the north wall, across the NE end of the trench, and onto the south wall, where it bifurcates, and continues part way up the south wall of the trench within Units 5 and 6 (Figure 10). The lower branch accommodated 68 cm, and the upper accommodated 74 cm of offset, so the total maximum offset on the lower fault in the south wall was approximately 1.4 m (Figure 10c, right). Thus, the maximum offset on the lower fault in the south wall was about one half the maximum offset of this fault in the north wall. The offset in the south wall markedly decreased upward and appeared to die out part way up the hinge of the syncline, within Units 5 and 4 (Figure 10, right). The upper branch was likely active during the 1999 earthquake based on abruptly truncated roots. The lowest branch is parallel to layering within Unit 5 (Figure 10b, right). We have no evidence to determine whether this branch was active or dormant during the 1999 earthquake.

3.2.2. Fault-Related Folds

Considering the south wall of the trench (Figures 10, right, and 11b), we see that several sedimentary layers define a highly asymmetric syncline in the footwall block of the upper main fault (U). Unit 6 near the top of the section in the hanging wall is horizontal in the face of the first (top) bench of the trench, turns downward sharply adjacent to the fault U, and is truncated. The syncline begins beneath the upper main fault U, where Unit 6, for example, continues as a vertical stratum (Figure 10, right). It continues as a horizontal layer within the base of the trench (Figure 11b). Thus, the syncline has an essentially vertical limb and a horizontal limb. The lower main fault has had less slip than the upper one, and it offsets some of the units near the hinge of the syncline.

In the north wall of the trench, the sedimentary layers are deformed into a highly asymmetric anticline in the hanging wall of the lower main fault (L) (Figures 10, left, and 11a). One limb of the anticline in the north wall is vertical to slightly overturned. The upper limb is nearly horizontal. Units 8 and 7 and part of Unit 6 are all tightly folded in the anticline. The wedge-shaped mass of gravel of Unit 8 is a tight anticlinal hinge. The gravel is in conformable contact with Unit 7, which wraps around the tight hinge in the gravel. Unlike in the south wall, there are both an intact synclinal hinge and an intact anticlinal hinge in the north wall.

3.2.3. Detailed Mapping of Medium-Sized and Small Faults

The lines showing fault traces in Figure 10c all represent fault traces, but the activity of the small faults, especially, is unknown for some of them. It was not a simple matter to determine which faults were active and which faults were dormant during the 1999 Chi-Chi earthquake (Figure 11). We emphasize, though, that the criteria are not all definitive, so the inferences about activity of the faults are tentative. The criteria are as follows (see Huang [2006] for examples): (1) If a fault breaks through the topsoil at the ground surface, the fault was active in 1999. (2) If a fault offsets any of the following markers, the fault formed or reactivated during the 1999 earthquake: (a) Roots circled by bluish gray stripes, which are the products of chemical reaction of the roots (Figure S1 in the supporting information). (b) Mottled stripes, which are normal to bedding and might well represent leaching (Figure S2). (c) Filled planar fractures. (3) If a fault trace was crossed by one

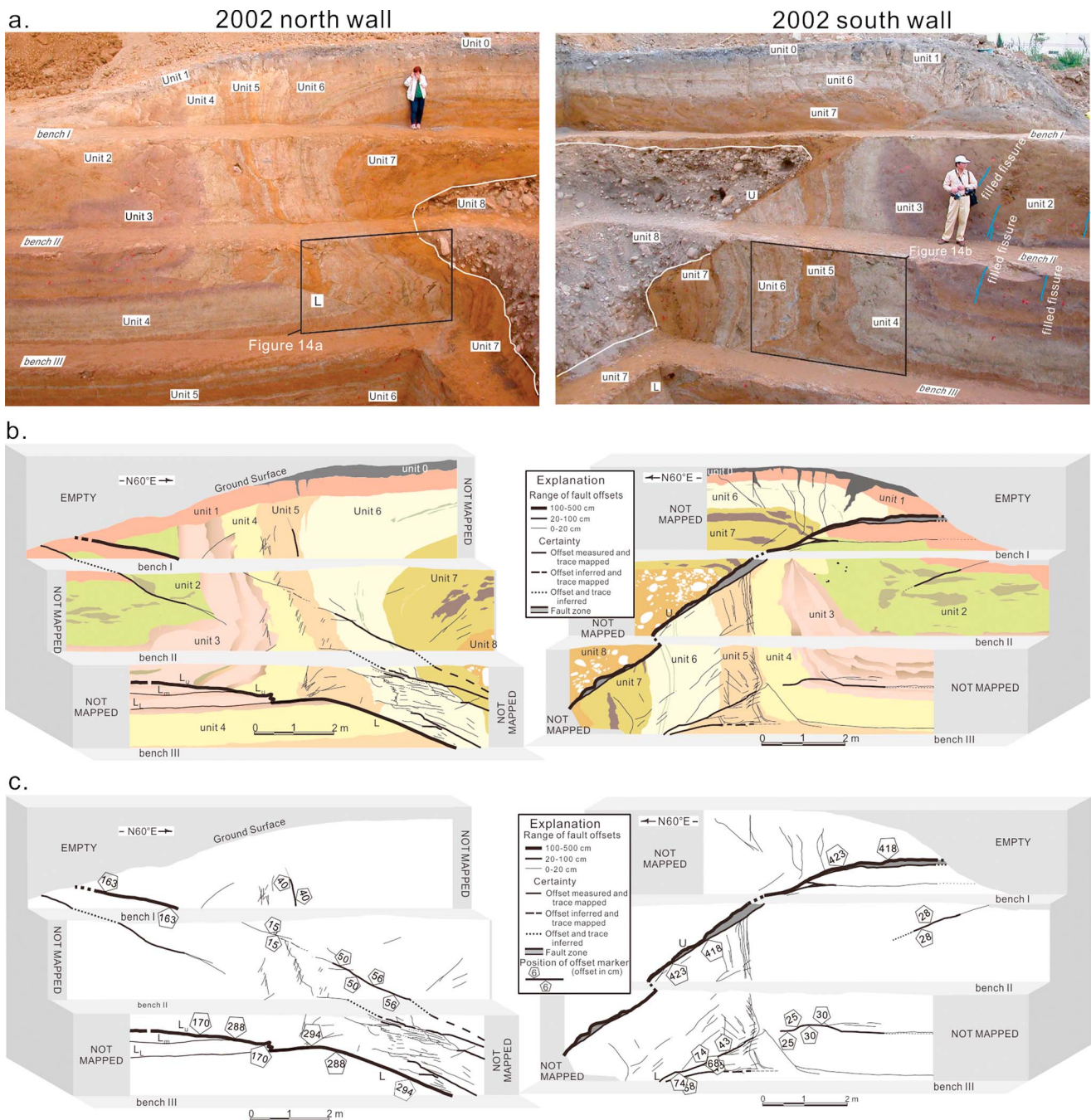


Figure 10. The 2002 north and south walls of the Chushan trench. Stratigraphic units are described in Figure 9. (a) NE end of walls of Chushan trench. The contact between Unit 7 and Unit 8 is highlighted in white lines (photography by Wei-Hsiung Lin, Taiwan Central Geological Survey). (b) Map of same area of north wall (left). Map of same area of south wall (right). (c) Maps of fault traces. The apparent slips measured on the main faults are indicated with a number (in centimeter) in paired pentagons that show positions of offset markers on the faces.

of the diagnostic markers but the marker is clearly not offset, the fault trace was mapped as dormant during the 1999 earthquake. (4) Finally, if all else failed, simple judgment was used to estimate whether a fault was dormant or active in 1999. For example, if a fault trace was well defined but there were no indicator of recent offset, the fault was still mapped. Perhaps the most important thing to note about the medium-sized and small faults is that those that were active during the Chi-Chi earthquake are less abundant in the south face, where the topographic profile is semiparabola-like, than in the north face, where the topographic profile is monoclinial (Figures 11 and 12a).

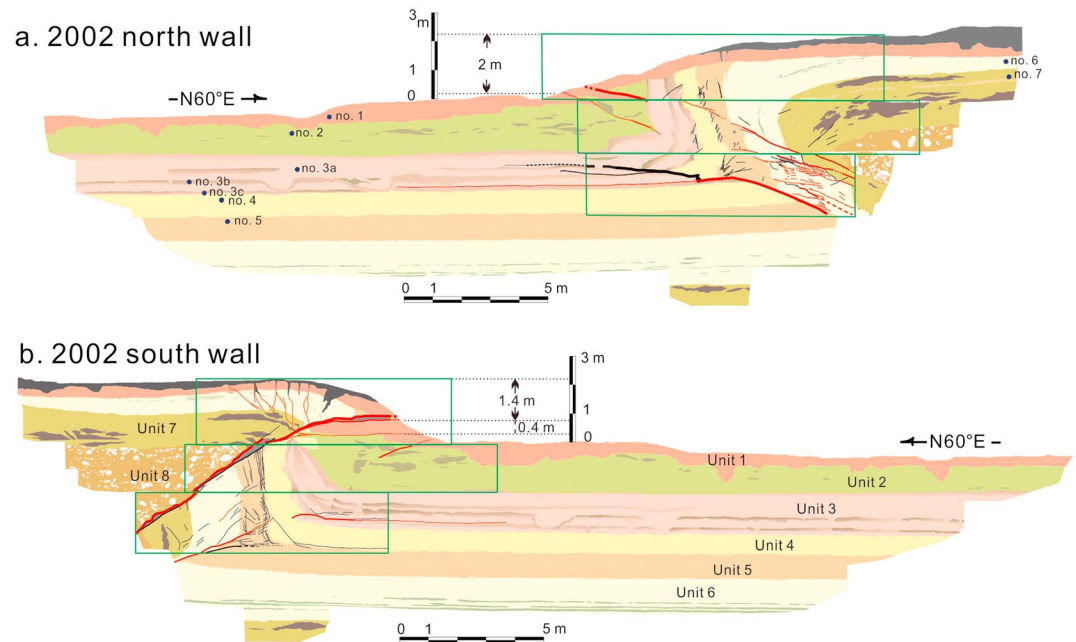


Figure 11. Profiles of the ground surface and cross sections of (a) north wall and (b) south wall of Chushan trench (modified from *Chen et al.* [2007]). Thicknesses of red and black lines indicate different offsets on faults: The thicker the line, the larger the offset. Faults in red were judged to have been active during Chi-Chi earthquake. Faults in black were dormant. Faults in areas bounded with rectangles are shown in detailed maps in Figure 10b and 10c. Soil samples no. 1 to 7 in Table 1 are labeled on the locations where they were collected.

3.2.3.1. Medium-Sized Faults

Very clear examples of medium-sized faults are shown in Figure 13, which shows the NE end of the face above the third bench of the north wall of the trench (Figure 10, left). The trench was expanded after the photograph in Figure 10a (left) was taken, so the structural expression on Figure 13 is somewhat different from that shown in Figure 10a (left). Medium-sized faults are defined as faults with apparent slip and length ranging from tenths of a meter to 2 m. Details of many of the medium-sized faults, as well as many small faults, with up to 20 cm of offset, are shown in maps in Figures 10c and 14. The medium-sized and small faults are common within the subvertical fold limb on both walls (Figures 10 and 14). The medium-sized faults and many of the small faults were strongly preferentially oriented parallel to the traces of the main faults. Some of the small faults, though, have various orientations.

Several discontinuous, medium-sized faults in the north wall (Figure 10c, left) appear to be coplanar with the upper main fault in the south wall (Figure 10c, right). The fault segments in the face above the second bench have decreasing stratigraphic separations of 56 cm, 50 cm, and 15 cm from bottom to top, according to Figure 10c (left). Particularly, interesting are medium-sized faults on the north wall that affect Units 1 and 2 (Figure 10, left). They are interesting in part because their traces terminate downward. One of them, exposed on the face of the first bench, shows a separation of 1.63 m. It cuts through the topsoil and therefore was active in 1999. Another one, on the face of the second bench, also cuts through the topsoil, with a separation of about 30 cm near the ground surface. A similar medium-size fault that terminates downward and was active in 1999 was observed in the south wall, on the face of the second bench, in front of the semiparabola-like toe (Figure 10, right). Its separation is 28 cm at shallow depth and decreases upward and downward.

We can estimate the cumulative offset of the parallel, medium-sized faults in the north wall by summing their offsets. We exclude the offset of the larger, main lower fault in the north wall because it may have reactivated but slipped only a few centimeter along its lower branch in 1999. Starting above the main fault, we have stratigraphic offset measurements on medium-sized faults of 20 cm, 60 cm, 25 cm, 95 cm, and 56 cm (Figure 14a). The value of 56 cm is an estimate of the medium-sized fault within the soil Unit 7 shown in dashed line in Figure 14a. We have a cumulative offset of 2.56 m. The apparent dip of the faults was 27°, so the offsets correspond to a throw (i.e., vertical component of movement), locally, of approximately 1.2 m. It is at least half a

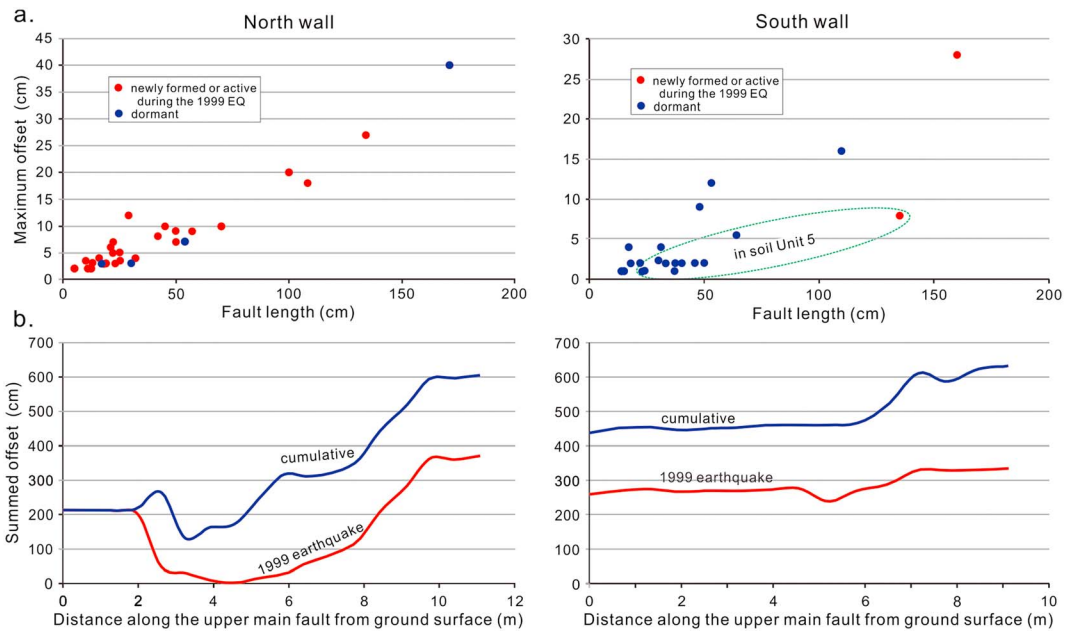


Figure 12. Fault offset on the 2002 exposures of the Chushan trench. (a) Maximum offset versus fault length for medium sized and small faults. (b) Plots of sums of projected fault offset along the upper main fault.

meter less than the throw produced there by the Chi-Chi earthquake. The faults, of course, do not extend through to the ground surface. Furthermore, we have discounted the slip on the main fault as well as all the small faults, so this computed value of throw is minimal for the faults in the north wall of the trench that were active in 1999.

3.2.3.2. Small Faults

Most of the faults in the subsurface structure fall into the category of small faults, the traces of which range over an order of magnitude from a few hundreds to a few tens of a meter and the apparent slip of which ranges over more than an order of magnitude from 1 to 20 cm. The lengths of traces of the smaller faults are generally short enough to be exposed on a single face of a bench.

There is a cluster of small faults between the lower main fault and a medium-sized fault exposed in the steep to overturned limb of the anticline in the north wall of the trench (Figures 10, left, and 14a). They were visible

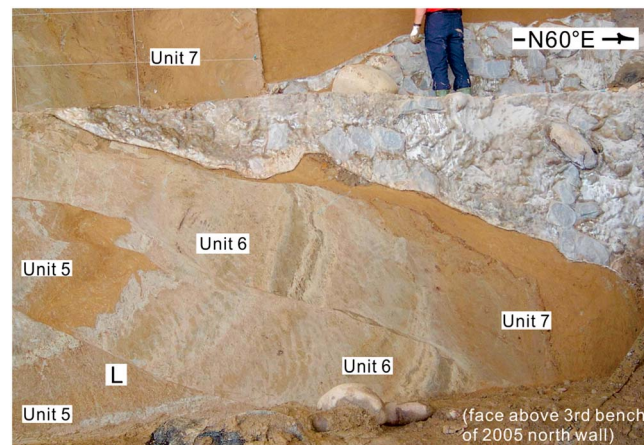


Figure 13. Detailed view of the NE end of the third bench of the 2005 north wall after the surface had been prepared for a plastic peel. The lowest of the two obvious faults is the lower main fault, identified as "L" in the text. It placed Unit 6 in lateral contact with Unit 5. The fault above, between two blocks of Unit 6, is termed medium-sized fault in the text.

mainly in Unit 6, light gray sandy, clayey silt. This unit has well-defined layering and laminations shown in the lower right in Figure 10a (left). The traces of the small faults were made visible by offsets of thin darker sandy layers in prepared faces in the trench; otherwise they might have been undetected. The small faults accommodate the same sense of shearing as the main faults. They are all reverse faults. The small faults in the cluster are subparallel, and their traces plunge 25° to 35°NE, roughly parallel to the main fault and medium-sized faults. The amount of offset on the small faults ranges from 1 to 20 cm, but offsets of 2 to 8 cm are most common. They accomplish significant average thinning of Units 4, 5, and 6 in the limb of the anticline.

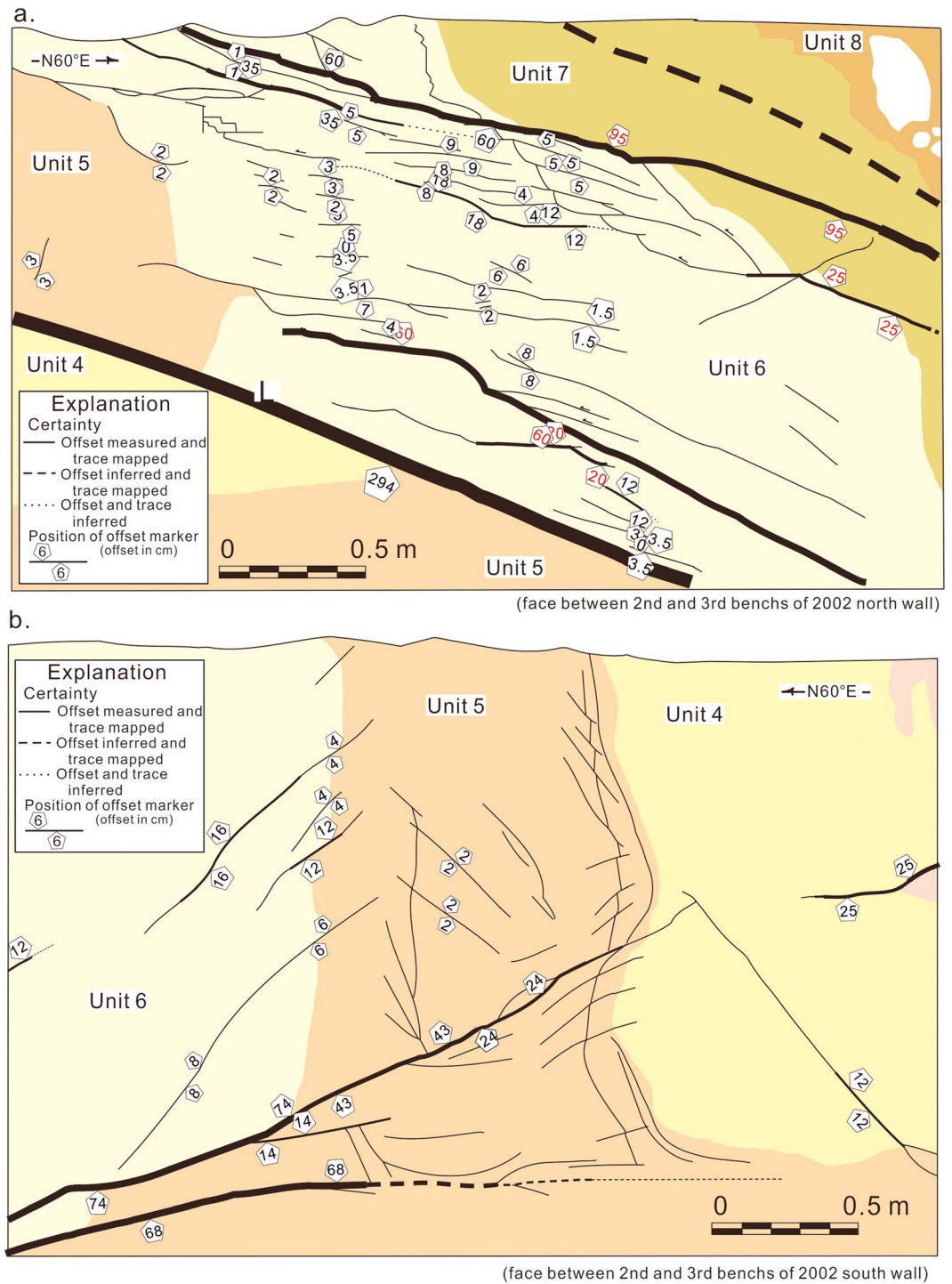


Figure 14. Detailed fault-trace maps. Widths of the fault traces indicate the size of the apparent slip: the thicker the line, the larger the apparent slip. Stratigraphic units defined in Figure 9. (a) Part of the 2002 north wall. Location is shown in Figure 10a (left). (b) Part of the 2002 south wall. Location is shown in Figure 10a (right).

There are also small faults in the steep limb of the syncline in the south wall of the trench. Although there are some small faults in Unit 6 in the south wall, they are more abundant in the brown clayey, sandy silt, Unit 5 (Figures 10, right, and 14b). In some places, we mapped three sets of fault traces with small offsets within Unit 5. The traces of one set of faults are vertical, subparallel to bedding. There were no markers to determine how much offset occurred on these faults. Two sets of fault traces offset mottled stripes a few millimeter to a few

centimeter and differ by their dip. The mottled stripes that were offset by the faults were roughly normal to layering. The two sets of faults also offset the layer-parallel fault traces in some places. These faults within Unit 5 have a distinctly smaller ratio of offsets to lengths (Figure 12a, right) like deformation bands described by *Fossen et al.* [2007].

The medium-sized and small faults have their maximum offset value scaling linearly with their length (Figure 12a), similar to earthquake faults reported by *Manighetti et al.* [2005], except those formed in Unit 5. Figure 12b (right) shows that summed offset occurring during the 1999 earthquake along the upper main fault increases from ~260 cm at the ground surface to ~330 cm at its lower end on the 2002 south wall. Figure 12b (left) shows a big gap of summed offset between 2 and 7 m down from the ground along a counterpart of the upper main fault on the 2002 north wall. The summed-offset inconsistency along the fault trace on either of walls may imply that ductile deformation took the place of brittle deformation in different degrees.

4. Structural Variations on Walls of the Chushan Trench

4.1. Topographic Profiles of the Escarpment

The topographic profiles of the escarpments formed in soft sediments at the leading edge of the thrust sheet that displaced during the 1999 Chi-Chi earthquake generally approach one of two classic forms [*Huang, 2006*]. The classic semiparabola-like profile (Figure 8a, right) is characterized by a ground slope that is very steep or vertical. A second classic form changes from a low slope at the leading edge to a higher slope and then back to a low slope (Figure 8a, left), that is the classic monoclinial profile. These two classic surface deformation profiles happened to occur on either side of the 14 m wide Chushan trench. There is a semiparabola-like profile at the ground surface in the south wall (Figures 8b and 10, right) and a smooth, rather open monoclinial profile at the ground surface in the north wall (Figures 8b and 10, left).

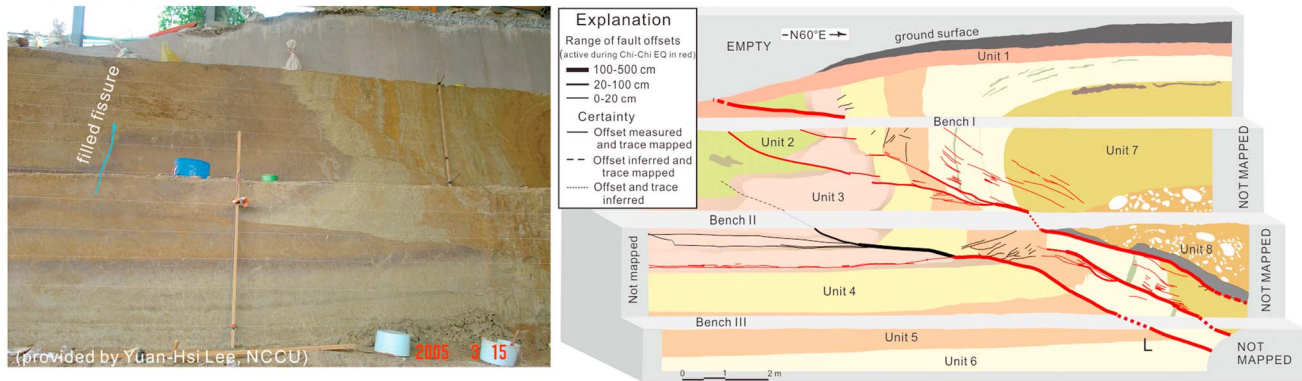
The semiparabola-like profile in the south wall of the trench (Figure 10a, right) is distinctly curved and is 4 to 5 m wide. The steeper part of the profile corresponds to the surface break of the upper main fault, where the topsoil in the hanging wall was carried about 2.4 m above the footwall (Figures 10, right, and 11b). The ground surface bulged upward about 1.5 m immediately behind the semiparabola-like profile above the main fault (Figure 11b). The bulging produced mode I fractures in the soil and sediment in the hanging wall of the upper fault. The fractures were opened as wedges and the gravel fill moved into the opening (Figures 11b and 10, right). In effect, the semiparabola-like profile was accomplished in part by “bending” of the hanging wall block bounded by the upper main fault (U) and the ground surface. The throw of the ground surface there was approximately 1.4 m (Figure 11b), consistent with the uplift expected from 2.4 m of slip on a 35° dipping fault. We note that the throw of the escarpment at the south side includes a step of about 0.4 m high, which probably existed prior to the Chi-Chi earthquake (Figure 11b).

The monoclinial profile in the north wall of the trench (Figures 8a and 10, left) is approximately 8 m wide and is somewhat irregular (Figure 11a) but is essentially an inclined plane, with most of the curvature at the top and bottom of the plane. This relatively smooth, monoclinial topographic profile occurs in the north wall of the trench, where the upper part of the subsurface structure is dominated by a highly asymmetric anticline rather than by a main fault (Figure 10a, left). The field mapping of faults that were active or probably active during the 1999 earthquake shows that, in fact, there was not a single large fault beneath the monoclinial profile, but rather a cluster of small and medium-sized faults (Figures 11a and 14a).

4.2. 2005 Exposure of the Trench

The trench was eroded severely 3 years after its first excavation, in particular on the northern wall. When the project of wall face preservation was began in 2005, a 1 m thick soil needed to be removed from the northern wall in order to make the faces flat and fresh again for peeling. Figure 15a shows the northern wall of the Chushan trench as documented in 2005. In comparison with Figure 10 (left), a variation of the subsurface structure is observed. The steep limb of the anticline above the lower main fault (L) is truncated by two medium-sized faults with a maximum separation of more than 1 m. It is likely the reason why the number of the small faults is significantly less in Unit 6 on this exposure compared to the 2002 exposure in Figures 10 (left) and 11a. The upper of these two faults bifurcates upward and then turns into a right-step en echelon feature toward the ground surface. That makes the Units 4, 5, and 6 look like unevenly stacked dominos on this part. Another interesting difference is that there is a newly discovered branch of the lower main fault

a. 2005 north wall



b. 2012 north wall

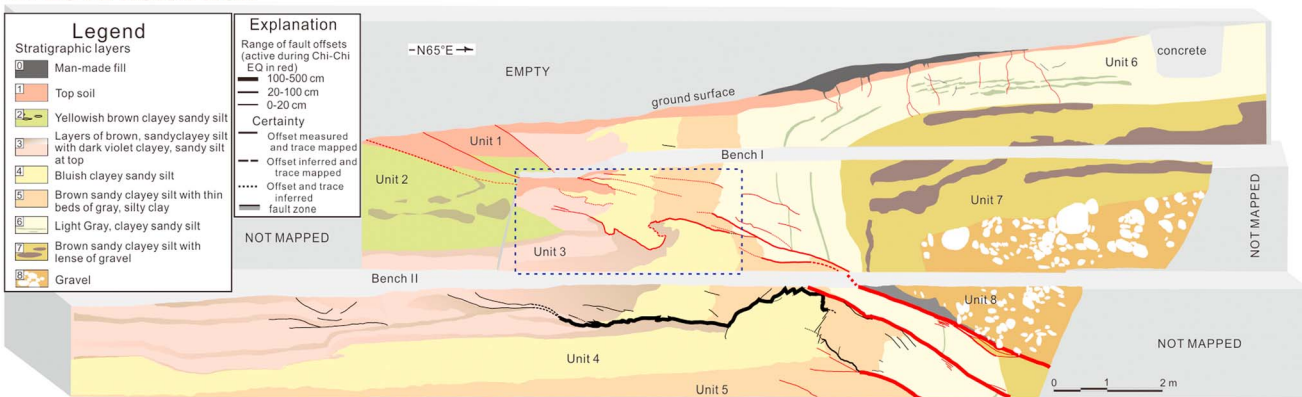


Figure 15. North walls of the Chushan trench in 2005 and 2012. (a) Photograph (left) and cross section of structures (right) of the 2005 north wall. The peeling project was ongoing while the photograph was taken. (b) Cross section of structures (up) and photograph (down) of the 2012 north wall. The dashed box circles an area which might be affected by post-earthquake effect attributed to an excavator (at middle left in Figure 8a).

likely associated with the flexure of the uppermost paleosol layer. This branch was dormant during the Chi-Chi earthquake because a steep filled fissure penetrated it without being displaced (Figure 15a, left).

4.3. 2012 Exposure of the Trench

Figure 15b shows the northern wall of the Chushan trench documented in 2012 located approximately 3 m north from the 2002 faces of the northern wall shown in Figure 10 (left) and approximately 2 m north from the 2005 faces shown in Figure 15a. In comparison with the 2002 exposure (Figure 10, left), the differences are obvious including the truncation of the anticline, the flexure of Unit 4 in the footwall of the lower main fault, and the stacking blocks of Units 3, 4, and 5 on the steep limb of the anticline (Figure S3). The truncation

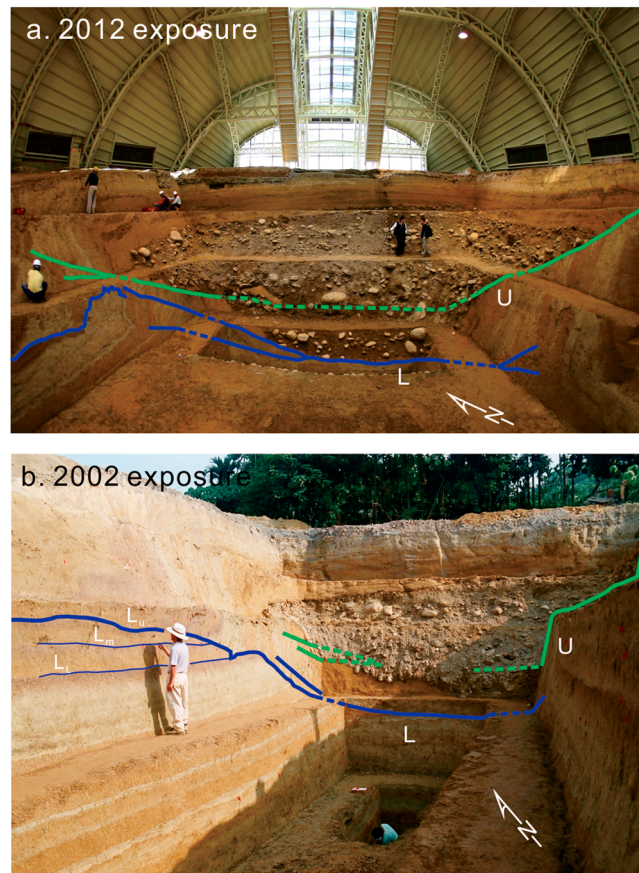


Figure 16. (a) Northeast view of the Chushan trench re-excavated in 2012 (photography by Yen-Chiou Lin, Taiwan Central Geological Survey). (b) Northeast view of the Chushan trench excavated at 2002 (photography by Wei-Hsiung Lin, Taiwan Central Geological Survey).

of the anticline in the 2012 exposure resembles the one in the 2005 wall with some slight variation. The flexure of Unit 4 in the northeastern end of the footwall suggests that the slip on the different branches of the lower main fault may have significantly varied between the two exposures (Figures 14b and 16). The irregularity of fault traces between Unit 3, Unit 4, and Unit 5 and the elevation inconsistency of the topsoil, Unit 1, on the face of the second bench (dashed box in Figure 15b, up) are likely attributed to post-1999 earthquake man-related disturbances. There are two normal faults with offset of about 1 m in total on a small face of the second bench perpendicular to the long axis of the trench. The two normal faults merge at a few centimeter above the second bench and appear to terminate downward. The formation of these normal faults and the irregularity of those fault traces likely resulted from the overload stress attributed to an excavator (at middle left in Figure 8b), which operated on the escarpment during the 2012 excavation. The affected depth, up to 2.5 m at the shallow ground (Figure 15b), is comparable to 4 times [Das and

Sobhan, 2013] the width, 60 cm, of the excavator winch. However, the irregularity of the lower main fault at depth of approximately 4 m might be due to the overprinting deformation induced by younger earthquake events.

4.4. Three-Dimensional Schematic Display

The geometric relationship between the two main faults along with their branches are revealed more clearly on the photographs in Figure 16 taken toward the eastern walls of the 2002 and 2012 exposures. The upper (U) and lower (L) main faults, traced in green and dark blue in the photographs respectively, run across the east wall from the north wall to the south wall and bifurcate in various places. Figure 17 shows a sketch of the faults in three dimensions based on the collated information of the trench walls. The excavations of the trench were at most 8 m in depth except a small rectangular hole (Figure 16b) down to 10 m in the footwall. Thus, the structures are inferred at depth, greater than 8 m.

Figure 17 illustrates the dramatic variation in the geometry of the upper main fault within the 17.5 m that separate the trench walls. It is not a trace of a single-plane fault on the 2002 south wall of the trench but an echelon trace array of an irregular, nonplanar fault on the 2002, 2005, and 2012 north walls. The lower main fault has a gap in Unit 4 on the 2002 south wall (Figures 10, right, and 11). The lower main fault turned into three branches in its upper part in the north walls and bifurcated in the lower part in both north and south walls. The fault plane between the upper and lower main faults shown in Figure 14 corresponds to the medium-sized faults that we observed at the axial plane of the syncline of Unit 2 in all the walls.

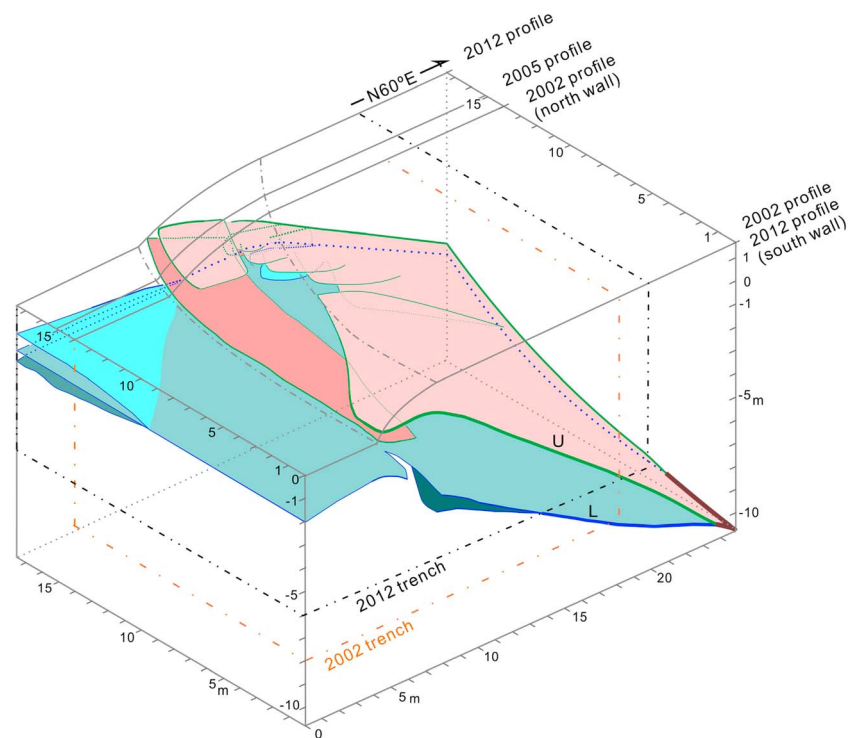


Figure 17. An illustrative three-dimension sketch of faults in Chushan trench. The upper main fault is labeled as U and the lower main fault is labeled as L. Widths of the fault traces also indicate the size of the slip: the thicker the line, the larger the slip. The dotted dashed lines indicate approximately the frame of the trench.

5. Discussion

5.1. Width Variation of the Deformation Zone at Tanliwun and Regulated Earthquake Fault Zone

The trend of the deformation zone at Tanliwun that roughly ran along the topographic contour line of 150 m reflected the intersection of a low-angle dip-slip fault with the ground surface (Figure 2). The width of the deformation zone apparently varied along strike and ranged from 15 to 70 m (Figure 3). We note that it was not a simple matter to determine the boundaries of the deformation zone. They were placed on the borderlines outward where there was no earthquake-induced deformation feature appearing on the ground surface, such as cracks, fractures, and folds, or the flex points of the ground-surface warp. The deformation zone was highly asymmetrical in reference to the toe of the escarpment and, most of all, much wider in the hanging wall than in the footwall (Figure 3). This phenomenon was largely recognized along the Chi-Chi earthquake deformation zone and consistent with results from a theoretical model proposed by *Huang and Johnson* [2010] and centrifuge experiments along with discrete element analysis conducted by *Chang et al.*, 2013, 2015. *Chang et al.*, 2013, 2015 simulated the surface and subsurface deformation induced by basement-detached reverse faulting through overburden sand. *Huang and Johnson* [2010] proposed an elastic-plastic model of fault slip propagation to explain the formation of deformation zones and estimate certain parameters to characterize the deformation zone.

The average widths of the entire deformation zone, of the hanging wall (w_{HW}) and of the footwall (w_{FW}) at Tanliwun were calculated by their individual areas divided by the length of the Chi-Chi coseismic escarpment. They are 36.8 m, 26.8 m, and 9.8 m, respectively (Table 2). The value of ratio of the w_{HW} and w_{FW} is approximately 2.7. According to the elastic-plastic model proposed by *Huang and Johnson* [2010], this value corresponds to a dip-slip fault with a dip angle of 31° (refer to Figure 8a in *Huang and Johnson* [2010]). This angle reasonably matches the angles of the major faults in the trench and is comparable to the fault angle of 24° [*Chen et al.*, 2007] derived from the location at the surface and in a borehole in the hanging wall (Figure 17). However, the w_{HW}/w_{FW} ratio of ~ 2.7 seems to apply to the deformation at the trench (Figures 11 and 18) to some degree, but it is far too small for the deformation zone across the A-A' profile in Figure 2, which w_{HW}/w_{FW} ratio is

Table 2. Width of Deformation Zone at Tanliwun

Deformation Zone, Dz	Area (m ²)	Width (m)		
		Average ^a	Max	Min
Entire Dz	35268.5	36.8	69.9	14.5–19.3
Dz in hanging wall	25838.5	26.8	65.2	~5
Dz in footwall	9430.3	9.8	33.3	~1

^aThe average widths are the areas divided by the length of the trace of Chi-Chi earthquake-induced escarpment, which is estimated as 962.7 m.

approximately 19.0. We think that the wider deformation zone in the hanging wall might result from slip on several branches of the dominant fault as shown in Figure 18. There are some arguments for that. The analysis on the structures in the Sanhu Yuan shows the consistency with thrusting in the Chushan trench, resulting from NE-SW compression. According to the model proposed by *Huang and Johnson* [2010], a value of ~19.0 for the ratio, w_{HW}/w_{FW} , corresponds to a dip angle of 13° for a dip-slip fault. Such a small angle does not seem reasonable for the geological setting at the Tanliwun area. Furthermore, there was a broad gap of ~22 m without any discernible deformation between the trench site and the Sanhu Yuan. *Chang et al.* [2015] defined the extent where the fault-induced surface deformation profile slope exceeds 1/150, i.e., ~0.38°, as affected width. As they indicated, the buildings that experienced an angular distortion of 1/150 would be expected to suffer considerable structural damage. The angular distortion is defined as the ratio of $\Delta S_{T(ij)}$ to L_{ij} , where ΔS_T and L_{ij} are differences in total settlement between any two points and distance between points i and j , respectively. According to their results (refer to Figure 28 in *Chang et al.* [2015]), the width of a fault-induced affected zone on the ground surface is predicted as ~24 m under a similar geological setting as the Tanliwun area, which is covered by 15.8 m thick unconsolidated sediment (Figure 18). This affected width, 24 m, is only about one third of the width, ~70 m, of the Chi-Chi deformation zone across the A-A' profile in Figure 2. We note that the experimental and numerical models of *Chang et al.* [2015] all started with a uniform-thickness overlaid material unlike the Tanliwun area, where the overlaid unconsolidated sediment varies significantly in thickness across the Chi-Chi deformation zone (Figure 18). In addition, shear planes and zones of fault gouge were observed in the Pliocene rocks of borehole no. 2 in the hanging wall of the dominant fault, which displaced Pliocene rocks over young alluvium layers. *Perrin et al.* [2015] suggested that the tip splay faults that branch off a main fault would form the most recent damage zone. Thus, we suggest that this wider deformation zone is attributed to the extra effect of slip on

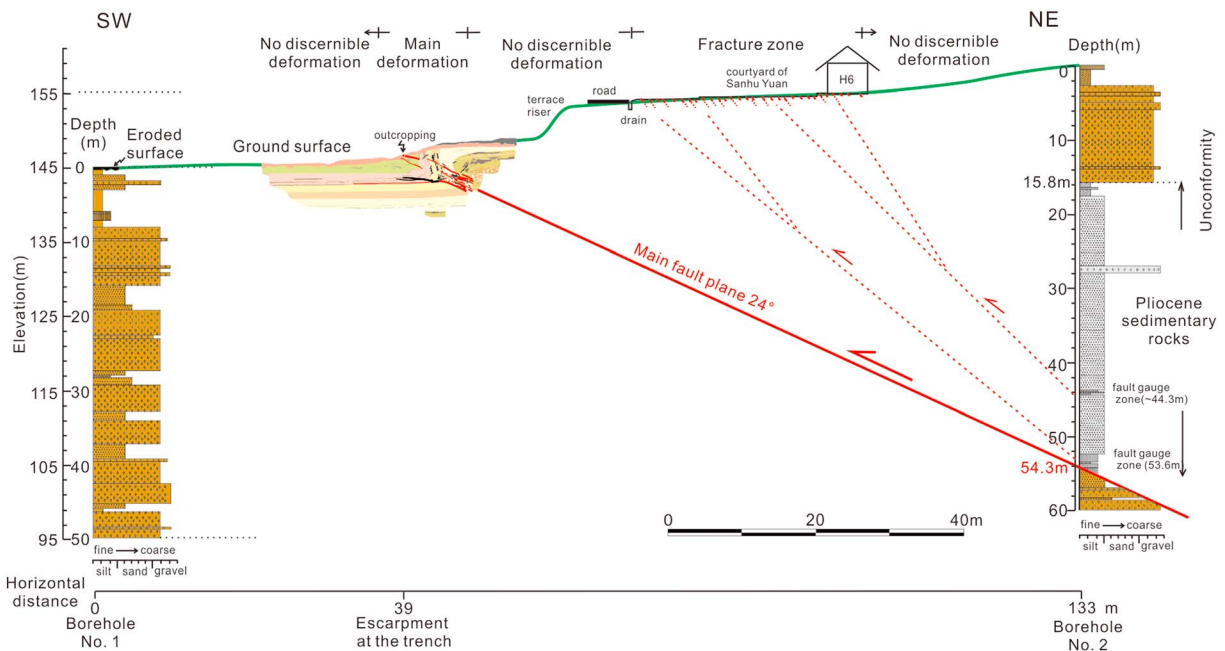


Figure 18. Cross section of the Chi-Chi earthquake-induced deformation zone at Tanliwun. See location in Figure 2.

secondary faults branching from the dominant fault at several tens of meters depth. We also argue that those uncommon locations with a wider deformation zone in the footwall (for example, location G in Figure 2) might also result from slip on branches of the dominant fault.

An Earthquake Fault Zone of the Chelungpu fault that was reactivated during the 1999 Chi-Chi earthquake was defined by the *Taiwan Central Geological Survey [TCGS]* [2014]. Considering the asymmetry and overall width extent of the Chi-Chi deformation zone, the zone coverage was determined as 200 m in the hanging wall and 100 m in the footwall relative to the Chi-Chi coseismic main fault trace or the toe of the coseismic escarpment. However, based on our observations, this zone coverage of 300 m in width is far too wide for the Tanliwun area (Figure 2 and Table 2), and probably for the entire 25 km long southern segment of the Chi-Chi rupture, south of Chuoshui River to the rupture southern termination. Because such an Earthquake Fault Zone brings major constraints to the public more for highly populated countries such as Taiwan, we suggest that the local characteristics of the coseismic deformation zone shall be taken into consideration and define an earthquake fault zone coverage accordingly.

5.2. Factors Responsible for the Differences in Deformation Patterns at the Trench

5.2.1. Difference in the Surface Deformation Profiles

The topographic profiles of the trench were semiparabola-like on the 2002 south wall and monoclinical on the 2002 north wall. Our observation of the structures on the walls shows that the parabolic topographic profile likely resulted from the breaking-through upper main fault, which slid along the ground surface for a couple of meters, whereas the monoclinical profile more likely resulted from a “ductile shear zone,” which was scale-dependent and where the deformation was induced by slip on multiple small faults at shallow depth. The latter scale-dependent ductile deformation can occur in soils [Fossen, 2010]. Huang [2006] also showed that the monoclinical ground surface generated by slip on several buried small faults could be similar to the surface deformation generated by slip on a single blind large fault. This finding, though, makes it difficult to uniquely predict the subsurface structures based on the morphologic shape of the deformed ground surface. However, it also implies that change in the escarpment morphology from the south wall to the north wall may depend on the depth of the upper tip of the relevant main fault or an equivalent blind large fault [Huang, 2006]. When a reverse fault does not break through the overlying soil but is close enough to the ground surface, such as in the south wall, fault slip tends to induce a monoclinical surface deformation profile. When the fault breaks through the soils and even slides along the ground for some distance as observed in the south wall, the ground-surface profile tends to become semiparabola-like. We note that the overlying geomaterials have to be soils or materials with similar mechanical properties; otherwise, it may result in a different scenario. For example, in the case of consolidated sedimentary rock, the overlying part of the hanging wall likely collapses and falls down into pieces of rock blocks after the hanging wall thrusts over and onto the footwall.

5.2.2. Difference in the Main Structures in the North and South Walls

A common question addressed by most people who have visited the trench is why the structure in one side of trench wall is “so different” from the one in the other side in such a short distance. Before we deduce the possible factors responsible for the difference, we emphasize some important facts. First, the throw related to Chi-Chi earthquake faulting/folding and even the cumulative throw at the trench after several earthquakes are almost identical [Chen *et al.*, 2007]. Second, the thickness and composition of Units 2 to 7 were laterally almost uniform within the trench, probably including the gravel, Unit 8, as well. Thus, one hardly attributes the difference to the soil units. We have learned that the 1999 earthquake produced approximately 1.4 to 2.0 m of throw (Figure 11). It is instructive to compare the throw accommodated by the faults with the throw across the entire trench. Then, we can estimate how many earthquakes the trench records. The difference in the main structures in the north and south walls might not occur all during the single 1999 Chi-Chi earthquake. We can determine the throw by comparing the positions of soil units preserved in the hanging wall to the same units preserved in the footwall of the structure. In the following, we use the south wall as an example. The oldest unit in the trench is the gravel, Unit 8. Units 7, 6, and a wedge-shaped block of Unit 5 are in conformable contact with underlying units (Figures 10, right and 10b). Unit 6 is only partly preserved except where it is in contact with the block of Unit 5. The lower structural contact of the gravel on the face of the second bench is bounded by the upper main fault, which places Unit 8 over Unit 6. The conformable contact between Unit 7 and Unit 8 appears again in the borehole located a few meters away from the trench (Figure 2). According to the positions of the top of the gravel, the throw across the trench was approximately 7.0 m [Chen *et al.*, 2007]. Furthermore, matching the lower part of Unit 6 preserved in the hanging wall of the

trench south wall with the lower part of Unit 6 exposed at the base of the trench in the footwall leads to a throw of 7.0 m (Figure 10, left), showing that no earthquake occurred between the formation of the top contact of Unit 8 and the deposition of the lower part of Unit 6. In addition, ^{14}C dating of the layers provides a chronological framework for the development of the trench structures (Figure 9) [Chen *et al.*, 2003, 2007]. The age of Unit 6 is roughly between 3360–3155 calibrated (cal) years B.P. and 3250–2980 cal years B.P., suggesting that the throw of 7.0 m occurred during the last 3200 years. Since the 1999 earthquake produced approximately 1.4 to 2.0 m of throw (Figure 10, left), there has been 5.0 to 5.6 m of throw earlier within the Chushan structure during the previous 3200 years. Therefore, including the Chi-Chi earthquake, we can infer that there were at least 2 to 4 earthquakes recorded in the Chushan trench assuming the throw on older earthquakes is the same as throw in 1999. Chen *et al.*, 2003, 2007 suggested that the structure started to form after the deposition of Unit 4 because Units 4 to 7 on both sides of the syncline axis show the same sedimentary facies, thicknesses, and lithologic characters. However, their statement about constant thicknesses is unconvincing, as shown in Figure 10a and 9b. The thickness variation, though, might result from the cumulative deformation induced by the earthquakes.

To illustrate how the structures evolved and diversified at the trench, we perform the structure restoration for the north and south walls of the 2002 excavation shown in Figure 19. To do so, we make a general assumption that the elevation of the contact between Unit 6 and Unit 7 in the hanging wall is roughly the same in different stages. Crucial observations to distinguish multiple successive events are listed as follows: (1) the activity and separations of the faults during the Chi-Chi earthquake discussed earlier shown in Figures 11 and 10c, (2) the gentle flat ground surface on the trench site before the Chi-Chi earthquake, (3) filled fractures with an upper bound at two third of Unit 2 from its bottom and their upward converging pattern at the syncline on the 2002 south wall (blue lines in Figure 10a, right), (4) the fault-related fold of Unit 3 at the upper tip of the main lower fault on the 2005 north wall and a filled fracture penetrating the fold (Figure 15a), and (5) the small remnant of Unit 5 above the upper main fault and the remnant of Unit 4 in Unit 2 below the upper main fault on the 2002 south wall. The items 1 and 2 allow us to restore the structures on the 2002 walls (Figure 19a) to the structures prior to the Chi-Chi earthquake shown in Figure 19b. The items 3 and 4 allow us to restore the structures in Figure 19c to the structures in Figure 19d, prior to the penultimate earthquake. In particular, we observed that the filled fractures in Unit 2 have a maximum inclination of approximately 25° at the short limb of the syncline, while they are all almost vertical out of the strain-localized zone in the footwall (Figure 10, right). That indicates that the short limb of the syncline rotated $\sim 25^\circ$ and became vertical after the penultimate earthquake. Then, because part of Unit 4 is present at the lower part of Unit 2, a prepenultimate earthquake has to have occurred before the deposition of Unit 2. This observation leads us to restore the structures in Figure 19e to the structure (Figure 19f) for the third last earthquake. During this event, the upper main fault appeared and broke through the paleo-ground surface in the south wall. It displaced Unit 4 onto Unit 3. After restoring the displacement, we can see an identical monocline with a throw of ~ 3.5 m on either of the walls. It implies at least one more earthquake to produce the monocline. Thus, we infer that the event of the third last earthquake was a crucial step at which the monocline started to evolve into two different forms and at least four earthquakes recorded in the Chushan trench.

Regarding the difference in the main structures in the 2002 north and south walls, it is likely due to a combined contribution, including the effects of the inherited structure, the bend of the dominant fault, and the coseismic slip during the contributing earthquakes. The subsurface main structure of the trench started to diversify from a monocline after the third last earthquake. The geometrical heterogeneity of the new faults, which developed across the monoclinical fold during the last three earthquakes, added the variation into the fold and resulted in the difference of the fault-related folds in the north and south walls of the 2002 trench. These new faults, especially the upper (U) and lower (L) main faults, are likely the branches of the dominant fault beneath the trench, which generated the monocline. Our observation on the fractures and cracks in the Sanhu Yuan indicates that the coseismic horizontal slip direction of faulting during the Chi-Chi earthquake was southwestward. The SW direction closely matches the horizontal slip on the Chi-Chi surface rupture determined by Lee *et al.* [2003] and a GPS displacement vector ~ 3 km southeast of the trench site, while most of the Chi-Chi coseismic GPS displacement vectors along the Chi-Chi surface rupture were oriented northwestwards [Yu *et al.*, 2001]. The trend of the Chi-Chi coseismic escarpment changed azimuth just north of the trench site (location B, Figure 2). It likely implies that the strike of the relevant fault had an abrupt change. Furthermore, our observations suggest that the upper and lower main faults were active during the Chi-Chi

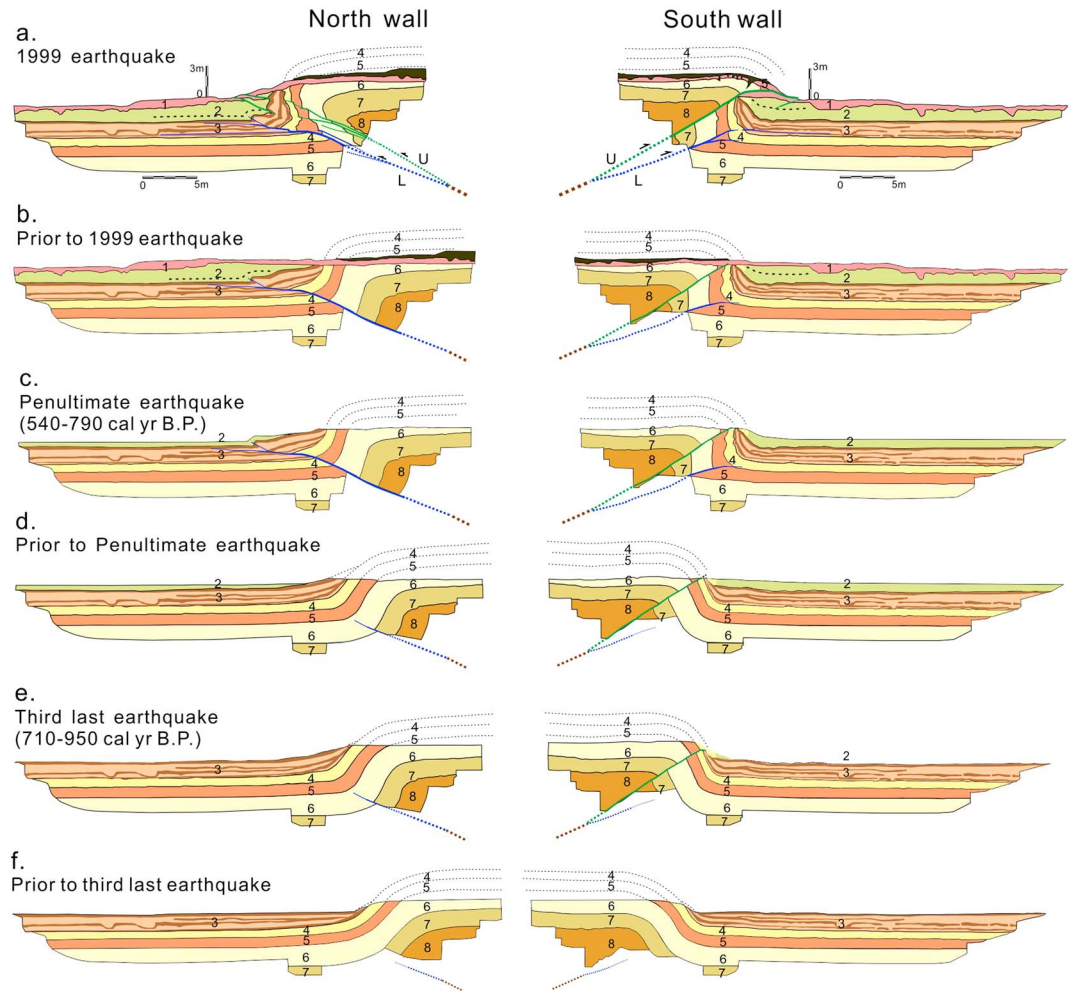


Figure 19. Progressive evolution of the structures on the 2002 south and north walls of the Chushan trench. The upper fault in green and lower main fault in blue are labeled as U and L, respectively. The stripping layers are shown in dotted lines. The radiocarbon age constraints of the paleoearthquakes refer to *Chen et al.* [2007].

earthquake and the upper main fault slipped much more than the lower main fault. Therefore, we suspect that the occurrence of the upper main fault and the slip partitioning on the two faults with different slip ratios might relate to the slip direction during different earthquakes. While the slip direction was oriented southwestward, most of the slip likely tended to occur on the upper main fault (third last earthquake and Chi-Chi earthquake; Figure 19e and 19a). While the slip direction was oriented westward or northwestward, most of the slips might tend to occur on the lower main fault (penultimate earthquake; Figure 19c). Such a phenomenon might result from the difference in the strikes of the overall fault planes.

6. Summary and Conclusions

We did detailed mapping on the surface and subsurface deformation in and near the Chushan trench, and integrated relevant information, including Chi-Chi earthquake rupture maps at a scale of 1:1000 at the Tanliwun area, two well logs, dated soils at the trench, in order to document and elucidate the heterogeneous structures of the 1999 Chi-Chi earthquake, thrust termination at Tanliwun, central Taiwan. The surface deformation zone characterized by a 0.5 to 2 m high escarpment has a significant variation in width, ranging from 15 to 70 m and is highly asymmetrical in reference to the toe of the escarpment. Commonly, the deformation zone was much wider in the hanging wall than in the footwall. Such a large variation in width of the surface deformation zone likely resulted from the effect of secondary faults branching from the dominant fault at several tens of meters depth.

Exposures in the Chushan trench, excavated across the earthquake ground rupture, show that on the one hand, the heterogeneous structure of a fault-related fold, and on the other hand, strikingly different surface deformation profiles on either side of the 14 m wide trench, which do not reflect in any obvious way the subsurface structure. The shape of the surface deformation profile was likely controlled by the depth of the relevant fault tip. The variation on the main fault-related folds in the trench walls seems due to the geometrical heterogeneity of the new faults, which developed across a preexisting monocline during the last three earthquakes. These new faults are likely the branches of the dominant fault beneath the trench, which generated the monocline. The geometrical heterogeneity of these faults might be mainly attributed to the bend of the dominant fault just north of the trench, and the coseismic slip during last three earthquakes.

Acknowledgments

This research was supported by the Department of Earth and Atmospheric Sciences, Purdue University, and would not have been possible without the generous and enthusiastic efforts of the Active Tectonics Division, Taiwan Central Geological Survey. In particular, we wish to thank Arvid M. Johnson, Professor Emeritus of Purdue University; Wei-Hsiung Lin, former Section Chief in Active Tectonics Division, Taiwan Central Geological Survey; and Section Chief Chi-Shyong Hou, surveyor Yen-Chiou Lin, and surveyor Tung-Sheng Shih, and technician Yin-Hao Chou in the Department of Civil Engineering, National Taiwan University. We thank Maryline Le Béon for critical comments that helped to improve the manuscript. We also thank Robert S. Yeatts, Stephane Dominguez, and an anonymous reviewer for their comments and time. Readers are welcome to contact the corresponding author for any inquiry regarding the present study.

References

- Angelier, J., et al. (2000), Geological knowledge and seismic risk mitigation: Insights from the Chi-Chi earthquake, Taiwan, in *Proceedings of International Workshop on Annual Commemoration of Chi-Chi Earthquake*, vol. 1, edited by C. H. Loh and W. I. Liao, pp. 13–24, National Center for Research on Earthquake Engineering, Taiwan.
- Boncio, P., P. Galli, G. Naso, and A. Pizzi (2012), Zoning surface rupture hazard along normal faults: Insight from the 2009 *M_w* 6.3 L'Aquila, central Italy, earthquake and other global earthquakes, *Bull. Seismol. Soc. Am.*, *102*(3), 918–935, doi:10.1785/0120100301.
- Bryant, W. A., and E. W. Hart (2007), *Fault-rupture Hazard Zones in California: Alquist-Priolo Earthquake Fault Zoning Act With Index to Earthquake Fault Zone Maps*, *Spec. Publ.*, vol. 42, 50 pp., California Geological Survey, Sacramento, Calif.
- Chang, Y. Y., C. J. Lee, W. C. Huang, W. J. Huang, M. L. Lin, W. Y. Hung, and Y. H. Lin (2013), Use of centrifuge experiments and discrete element analysis to model the reverse fault slip, *Int. J. Civil Eng.*, *11*(2), 79–88.
- Chang, Y. Y., C. J. Lee, W. C. Huang, W. Y. Hung, W. J. Huang, M. L. Lin, and Y. H. Chen (2015), Evolution of the surface deformation profile and subsurface distortion zone during reverse faulting through overburden sand, *Eng. Geol.*, *184*, 52–70.
- Chen, C. H. (1977), Some stratigraphic problems of the Hsuehshan Range of Taiwan, *Proc. Geol. Soc. China*, *20*, 61–70.
- Chen, W. S., et al. (2001a), 1999 Chi-Chi earthquake: A case study on the role of thrust-ramp structures for generating earthquakes, *Bull. Seismol. Soc. Am.*, *91*(5), 986–994.
- Chen, W. S., L. S. Lee, C. C. Yang, L. H. Liu, and Y. C. Chen (2003), Paleoseismic study of the Chelungpu fault in the Chushan, Nantao County, *Field report of Central Geological Survey, Taiwan*, 92–7, Project no. 5226902000–03–9201.
- Chen, W. S., et al. (2007), Late Holocene paleoseismicity of the south part of the Chelungpu fault in central Taiwan: Evidence from the Chushan excavation site, *Bull. Seismol. Soc. Am.*, *97*(1B), 1–13.
- Chen, Y. G., W. S. Chen, J. C. Lee, Y. H. Lee, C. T. Lee, H. C. Chang, and C. H. Lo (2001b), Surface rupture of 1999 Chi-Chi earthquake yields insights on active tectonics of central Taiwan, *Bull. Seismol. Soc. Am.*, *91*(5), 977–985.
- Chou, J. T. (1971), A sedimentologic and paleogeographic study of the neogene formations in the Taichung region, western Taiwan, *Pet. Geol. Taiwan*, *9*, 43–66.
- Chou, J. T. (1973), Sedimentology and palaeogeography of the Upper Cenozoic System of western Taiwan, *Proc. Geol. Soc. China*, *16*, 111–143.
- Chou, J. T. (1980), Stratigraphy and sedimentology of the Miocene in western Taiwan, *Pet. Geol. Taiwan*, *17*, 33–52.
- Chou, J. T. (1999), Evolution of the cenozoic sedimentary basin in Taiwan, *Symposium on Review and View of Geological Researches in Taiwan in Twenty Century*(II), 1–78.
- Chou, J. T., and C. I. Yang (1986), Characteristics and oil gas storing potential of sedimentary basin, *Western Taiwan Pet. Quart.*, *22*(1), 2–25.
- Cotterell, B., and J. R. Rice (1980), Slightly curved or kinked cracks, *Int. J. Fract.*, *16*(2), 155–169.
- Das, B. M., and K. Sobhan (2013), *Principles of Geotechnical Engineering*, 768 pp., Cengage Learning, Stamford, Connecticut.
- Dong, J. J., C. D. Wang, C. T. Lee, J. J. Liao, and Y. W. Pan (2004), The influence of surface ruptures on building damage in the 1999 Chi-Chi earthquake: A case study in Fengyuan City, *Eng. Geol.*, *71*, 157–179, doi:10.1016/S0013-7952(03)00131-5.
- Fossen, H. (2010), *Structural Geology*, 463 pp., Cambridge Univ. Press, New York.
- Fossen, H., R. A. Schultz, Z. K. Sipton, and K. Mair (2007), Deformation bands in sandstone: A review, *J. Geol. Soc. London*, *164*, 755–769.
- Gilbert, G. K. (1907), The earthquake as a natural phenomenon, in *The San Francisco Earthquake and Fire*, *U.S. Geol. Surv. Bull.*, *324*, 1–13.
- Ho, C. S. (1988), *An Introduction to the Geology of Taiwan: Explanatory Text of the Geology Map of Taiwan*, 2nd ed., 192 pp., Ministry of Economic Affairs, R.O.C.
- Huang, C. Y., and Y. M. Cheng (1983), Oligocene and Miocene planktonic foraminiferal biostratigraphy of northern Taiwan, *Proc. Geol. Soc. China*, *26*, 21–56.
- Huang, W. J. (2006), Deformation at the leading edge of thrust faults, PhD dissertation, 435 pp., Purdue Univ., West Lafayette, Indiana, July.
- Huang, W. J., and A. M. Johnson (2010), Quantitative description and analysis of earthquake-induced deformation zones along strike-slip and dip-slip faults, *J. Geophys. Res.*, *115*, B03408, doi:10.1029/2009JB006361.
- Huang, W. J., Z. Y. Chen, S. Y. Liu, C. W. Lin, and H. C. Chang (2000), Surface deformation models of the 1999 Chi-Chi earthquake between Tachiachi and Toupian Kengchi, central Taiwan [in Chinese], *Spec. Publ. Central Geol. Surv.*, *12*, 63–87.
- Johnson, A. M., R. W. Fleming, and K. M. Cruikshank (1993), Broad belts of shear zones as the common form of surface rupture produced by the 28 June 1992 Landers, California, earthquake, *U.S. Geol. Surv. Open File Rep.*, *93–348*, 61 pp.
- Johnson, A. M., R. W. Fleming, and K. M. Cruikshank (1994), Shear zones formed along long, straight traces of fault zones during the 28 June 1992 Landers, California, earthquake, *Bull. Seismol. Soc. Am.*, *84*(3), 499–510.
- Johnson, A. M., R. W. Fleming, K. M. Cruikshank, and R. F. Packard (1996), Coactive fault of the Northridge earthquake—Granada Hills area, California, *U.S. Geol. Surv. Open File Rep.*, *96–523*, 66 pp.
- Johnson, A. M., K. M. Johnson, J. Durdella, M. Sozen, and T. Gur (2002), An emendation of elastic rebound theory: Main rupture and adjacent belt of right-lateral distortion detected by viaduct at Kaynasli, Turkey 12 November 1999 Duzce earthquake, *J. Seismol.*, *6*, 329–346, doi:10.1023/A:1020031324622.
- Kaneda, H., et al. (2008), Surface Rupture of the 2005 Kashmir, Pakistan, earthquake and its active tectonic implications, *Bull. Seismol. Soc. Am.*, *98*(2), 521–557, doi:10.1785/0120070073.
- Kelson, K. I., K. H. Kang, W. D. Page, C. T. Lee, and L. S. Cluff (2001), Representative styles of deformation along the Chelungpu fault from the 1999 Chi-Chi (Taiwan) earthquake: Geomorphic characteristics and responses of man-made structures, *Bull. Seismol. Soc. Am.*, *91*(5), 930–952, doi:10.1785/0120000741.

- Klinger, Y., X. Xu, P. Tapponnier, J. V. Woerd, C. Lasserre, and G. King (2005), High-resolution satellite imagery mapping of the surface rupture and slip distribution of the Mw ~7.8, 14 November 2001 Kokoxili earthquake, Kunlun Fault, northern Tibet, China, *Bull. Seismol. Soc. Am.*, *95*(5), 1970–1987, doi:10.1785/0120040233.
- Lawson, A. C. (1908), California earthquake of April 18, 1906: Report of the State Earthquake Investigations Commission, *Carnegie Inst. Washington Publ.*, *87*(1), 451.
- Lee, J. C., Y. G. Chen, K. Sieh, K. Muller, W. S. Chen, H. T. Chu, Y. C. Chan, C. Rubin, and R. Yeats (2001), A vertical exposure of the 1999 surface rupture of the Chelungpu fault at Wufeng, western Taiwan: Structural and paleoseismic implications for an active thrust fault, *Bull. Seismol. Soc. Am.*, *91*(5), 914–929.
- Lee, J. C., H. T. Chu, J. Angelier, Y. C. Chan, J. C. Hu, C. Y. Lu, and R. J. Rau (2002), Geometry and structure of northern surface ruptures of the 1999 Mw = 7.6 Chi-Chi Taiwan earthquake: Influence from inherited fold belt structures, *J. Struct. Geol.*, *24*, 173–192.
- Lee, Y. H., and Y. X. Shih (2011), Coseismic displacement, bilateral rupture, and structural characteristics at the southern end of the 1999 Chi-Chi earthquake rupture, central Taiwan, *J. Geophys. Res.*, *116*, B07402, 2011, doi:10.1029/2010JB007760.
- Lee, Y. H., M. L. Hsieh, S. D. Lu, T. S. Shih, W. Y. Wu, Y. Sugiyama, T. Azuma, and Y. Kariya (2003), Slip vectors of the rupture of the 1999 Chi-Chi earthquake, western Taiwan, *J. Struct. Geol.*, *25*, 1917–1931, doi:10.1016/S0191-8141(03)00039-7.
- Lee, Y. H., S. T. Lu, T. S. Shih, M. L. Hsieh, and W. Y. Wu (2005), Structures associated with the northern end of the 1999 Chi-Chi earthquake rupture, central Taiwan: Implications for seismic-hazard assessment, *Bull. Seismol. Soc. Am.*, *95*(2), 471–485, doi:10.1785/0120020170.
- Li, C. Y., Z. Y. Wei, J. Q. Ye, Y. B. Han, and W. J. Zheng (2010), Amounts and styles of coseismic deformation along the northern segment of surface rupture, of the 2008 Wenchuan Mw 7.9 earthquake, China, *Tectonophysics*, *491*, 35–58.
- Lin, A., and M. Nishikawa (2011), Riedel shear structures in the co-seismic surface rupture zone produced by the 2001 Mw 7.8 Kunlun earthquake, northern Tibetan Plateau, *J. Struct. Geol.*, *33*, 1302–1311.
- Lin, A., T. Ouchi, A. Chen, and T. Maruyama (2001), Co-seismic displacements, folding and shortening structures along the Chelungpu surface rupture zone occurred during the 1999 Chi-Chi (Taiwan) earthquake, *Tectonophysics*, *330*, 225–244.
- Lin, A., Z. Ren, D. Jia, and X. Wu (2009), Co-seismic thrusting rupture and slip distribution produced by the 2008 Mw 7.9 Wenchuan earthquake, China, *Tectonophysics*, *471*, 203–215.
- Lin, C., and H. F. Suen (2000), *In Witness of Chi-Chi Earthquake—The Causes of Damage and Countermeasures*, 923 pp., McGraw-Hill, Taiwan.
- Lin, C. W., H. C. Chang, S. D. Lu, T. S. Shih, and W. J. Huang, 2002. An introduction to the active faults of Taiwan with explanatory text of the active fault map of Taiwan, scale 1:500,000 [in Chinese with English abstract], *Special publication of the Central Geological Survey, MOEA*, *13*, 122 pp.
- Lin, C. W., Y. L. Lee, L. M. Huang, W. C. Lai, B. D. Yuan, and C. Y. Huang (2003), Characteristics of surface ruptures associated with the Ch-Chi earthquake of September 21, 1999, *Eng. Geol.*, *71*, 13–30.
- Manighetti, I., M. Campillo, C. Sammis, P. M. Mai, and G. King (2005), Evidence for self-similar, triangular slip distributions on earthquakes: Implications for earthquake and fault mechanics, *J. Geophys. Res.*, *110*, B05302, doi:10.1029/2004JB003174.
- Martosudarmo, S. Y., A. M. Johnson, and R. W. Fleming (1997), Ground fracturing on the southern end of Summit Ridge caused by the October 17, 1989 Loma Prieta, California earthquake, *U.S. Geol. Surv. Open File Rep.*, *97-129*, 43 pp., 5 plates.
- Ota, Y., M. Watanabe, Y. Suzuki, M. Yanagida, A. Miyawaki, and H. Sawa (2007), Style of the surface deformation by the 1999 Chichi earthquake at the central segment of Chelungpu fault, *Taiwan, J. Asian Earth Sci.*, *31*, 214–225.
- Ouchi, T., A. Lin, A. Chen, and T. Maruyama (2001), The 1999 Chi-Chi (Taiwan) earthquake: Earthquake fault and strong motions, *Bull. Seismol. Soc. Am.*, *91*(5), 966–976.
- Perrin, C., I. Manighetti, and Y. Gaudemer (2015), Off-fault tip splay networks: A genetic and generic property of faults indicative of their long-term propagation, *C. R. Geosci.*, doi:10.1016/j.crte.2015.05.002.
- Philip, H., and M. Meghraoui (1983), Structural analysis and interpretation of the surface deformations of the El Asnam earthquake of October 10, 1980, *Tectonics*, *2*(1), 17–49.
- Ren, J., G. Chen, X. Xu, S. Zhang, and C. Mao (2010), Surface Rupture of the 2008 Wenchuan, China, Earthquake in the Qingping stepover determined from geomorphologic surveying and excavation, and its tectonic implications, *Bull. Seismol. Soc. Am.*, *100*(5B), 2651–2659, doi:10.1785/0120090267.
- Rockwell, T. K., S. Lindvall, T. Dawson, R. Langridge, W. Lettis, and Y. Klinger (2002), Lateral offsets on surveyed cultural resulting from 1999 Izmit and Duzce earthquakes, Turkey, *Bull. Seismol. Soc. Am.*, *92*(1), 79–94.
- Rubin, C. M., K. Shieh, Y. G. Chen, J. C. Lee, H. T. Chu, R. Yeats, K. Mueller, and Y. C. Chan (2001), Surface rupture and behavior of thrust faults probed in Taiwan, *Eos Trans. AGU*, *82*, 565–569.
- Seed, H. B., R. J. Woodward, and R. Lundgren (1964a), Clay mineralogical aspects of the Atterberg limits, *J. Soil Mech. Found. Div. A.S.G.E.*, *90*(SM4), 107–131.
- Seed, H. B., R. J. Woodward, and R. Lundgren (1964b), Fundamental aspects of the Atterberg limits, *J. Soil Mech. Found. Div. A.S.G.E.*, *90*(SM6), 107–131.
- Shyu, J. B. H., K. Sieh, Y. G. Chen, and C. S. Liu (2005), Neotectonic architecture of Taiwan and its implications for future large earthquakes, *J. Geophys. Res.*, *110*, B08402, doi:10.1029/2004JB003251.
- Taiwan Central Geological Survey (TCGS) (1999a), Surface ruptures along the Chelungpu fault during the Chi-Chi earthquake, Taiwan, map at scale, 1:25000, Central Geol. Surv., Minist. of Econ. Affairs, Taipei.
- Taiwan Central Geological Survey (TCGS) (1999b), Report of the geological survey of the 1999 Chi-Chi earthquake [in Chinese], Central Geol. Surv., Minist. of Econ. Affairs, Taipei.
- Taiwan Central Geological Survey (TCGS) (2014), Regulated Earthquake fault zones of Taiwan – F0001 Chelungpu fault [in Chinese], Central Geol. Surv., Minist. of Econ. Affairs, Taipei.
- Tchalenko, J. S., and N. N. Ambraseys (1970), Structural analysis of the Dasht-e Bayaz (Iran) earthquake fractures, *Geol. Soc. Am. Bull.*, *81*(1), 41–60.
- Teng, L. S., Y. Wang, C. H. Tang, C. Y. Huang, T. C. Huang, M. S. Yu, and A. Ke (1991), Tectonic aspects of the Paleogene depositional basin of northern, *Taiwan. Proc. Geol. Soc. China*, *34*, 313–336.
- Treiman, J. A., K. J. Kendrick, W. A. Bryant, T. K. Rockwell, and S. F. McGill (2002), Primary surface rupture associated with the Mw 7.1 16 October 1999 Hector Mine earthquake, San Bernardino County, California, *Bull. Seismol. Soc. Am.*, *92*(4), 1171–1191.
- Villamor, P., et al. (2012), Map of the 2010 Greendale Fault surface rupture, Canterbury, New Zealand: Application to land use planning, *N. Z. J. Geol. Geophys.*, *55*(3), 223–230, doi:10.1080/00288306.2012.680473.
- Yu, S. B., L. C. Kuo, Y. J. Hsu, H. H. Su, and C. C. Liu (2001), Preseismic deformation and coseismic displacements associated with the 1999 Chi-Chi, Taiwan earthquake, *Bull. Seismol. Soc. Am.*, *91*(5), 995–1012.